11284–11303 *Nucleic Acids Research, 2019, Vol. 47, No. 21* *Published online 15 October 2019*
doi: 10.1093/nar/gkz901

A novel and translational role for autophagy in antisense oligonucleotide trafficking and activity

Joseph Ochaba, Andrew F. Powers, Kaitlyn A. Tremble, Sarah Greenlee, Noah M. Post, John E. Matson, A. Robert MacLeod, Shuling Guo and Mariam Aghajan*

Ionis Pharmaceuticals, Inc., Carlsbad, CA 92010, USA

Received April 19, 2019; Revised September 13, 2019; Editorial Decision September 30, 2019; Accepted October 01, 2019

ABSTRACT

Endocytosis is a mechanism by which cells sense their environment and internalize various nutrients, growth factors and signaling molecules. This process initiates at the plasma membrane, converges with autophagy, and terminates at the lysosome. It is well-established that cellular uptake of antisense oligonucleotides (ASOs) proceeds through the endocytic pathway; however, only a small fraction escapes endosomal trafficking while the majority are rendered inactive in the lysosome. Since these pathways converge and share common molecular machinery, it is unclear if autophagy-related trafficking participates in ASO uptake or whether modulation of autophagy affects ASO activity and localization. To address these questions, we investigated the effects of autophagy modulation on ASO activity in cells and mice. We found that enhancing autophagy through small-molecule mTOR inhibition, serum-starvation/fasting, and ketogenic diet, increased ASO-mediated target reduction *in vitro* and *in vivo*. Additionally, autophagy activation enhanced the localization of ASOs into autophagosomes without altering intracellular concentrations or trafficking to other compartments. These results support a novel role for autophagy and the autophagosome as a previously unidentified compartment that participates in and contributes to enhanced ASO activity. Further, we demonstrate non-chemical methods to enhance autophagy and subsequent ASO activity using translatable approaches such as fasting or ketogenic diet.

INTRODUCTION

Antisense oligonucleotides (ASOs) have been extensively developed for use as research tools and therapeutic agents that modulate gene expression through various cellular mechanisms (1,2). To improve chemical stability and pharmacological efficacy, ASOs are commonly synthesized with a phosphorothioate (PS) backbone and also contain sugar modifications that include but are not limited to 2′-*O*-methoxyethyl (MOE) or constrained ethyl (cEt) at the 2′-position of the ribose (2). An employed mechanism involves chimeric or 'gapmer' design ASOs, whereby residues at each terminus of the oligo are chemically modified and flank a central DNA region, enabling knockdown of their RNA target via direct sequence-specific cleavage mediated by the RNase H1 endonuclease (3). A major advantage of ASOs is their hydrophobicity and interactions with surface proteins which enables them to enter cells independent of nanoparticles, liposomes or conjugation to cell-penetrating peptides (4). For example, ASOs interact with receptors including stabilin and EGFR, which mediate ASO uptake through receptor-dependent endocytosis (5,6). Upon internalization, ASOs traffic through early endosomes (EE) within 10–30 min, transport to late endosomes (LEs) within 20–60 min, and ultimately reach the lysosome between 2 and 4 h (5). While differences in endocytic internalization and trafficking of ASOs may vary by cell-type, it is evident that after internalization only a small fraction of intracellular ASOs contribute to overall activity, as the majority of ASOs exist in non-productive compartments such as the lysosome. Thus, one strategy to increase the potency of oligonucleotide therapeutics is to enhance endolysosomal escape, which may also enable effective oligonucleotide activity in a broader range of cell types (7). Understanding the mechanisms by which ASOs traffic to and from various membrane-enclosed organelles is critical to understand the processes that ultimately lead to release and accumulation of ASO at target sites.

An important challenge for conceptualizing endolysosomal trafficking of ASOs is the reality that endocytosis is not an isolated pathway leading from the endosome to the lysosome, but rather a complex web of inputs and outputs from other trafficking cascades (8). One such pathway is macroautophagy (hereafter referred to as autophagy), which is a catabolic pathway that sequesters protein aggregates, damaged organelles, or intracellular pathogens in

*To whom correspondence should be addressed. Tel: +1 760 603 2481; Email: MAghajan@ionisph.com

double-membraned autophagosomes that fuse with lysosomes to achieve degradation (9,10). Autophagy functions to supplement cellular metabolism during periods of starvation, but also serves as a mechanism to dispose toxic species that would otherwise disrupt cellular homeostasis. Initiation of autophagy is suppressed by the mammalian target of rapamycin kinase complex 1 (mTORC1), whose activity is regulated by nutrient availability and cellular stress (11,12). Following mTORC1 inhibition, the ULK1 and Beclin1/VPS34 kinase complexes trigger the sequential recruitment of autophagy-related (ATG) proteins to nascent phagophores through a ubiquitin-like conjugation cascade that drives autophagosome formation (e.g. ATG5-12-16L) and cargo recruitment (e.g. ATG8/LC3). Active mTOR also functions to maintain cytoplasmic localization of transcription factor EB (TFEB), a critical transcription factor governing the expression of autophagy and lysosome-related genes. Under nutrient-rich conditions, mTORC1 directly phosphorylates and inhibits TFEB (13). Conversely, inhibition of mTORC1 leads to the dephosphorylation and nuclear translocation of TFEB, where it enhances transcription of CLEAR network genes, resulting in biogenesis and activation of autolysosomal machinery (14–16).

Previous work has invoked the idea that pharmacological modulation of autophagy might increase oligonucleotide distribution in cells, resulting in enhanced knockdown activity. Interestingly, it has been suggested that pharmacological modulation of autophagic processes might alter oligonucleotide efficiency, distribution, and activity (17–19). However, these studies inferred a role for autophagy in oligonucleotide uptake and trafficking based on experiments that used artificial lipid-based delivery systems which have been reported to not only induce non-physiological electrostatic-mediated endosomal escape but also result in increased autophagosome production and autophagy induction (20–23). The effects of lipid-based delivery on autophagy and endo-lysosomal trafficking not only complicate these previous interpretations regarding the effects of autophagy on oligonucleotide activity, but also question their relevance to physiological settings involving naked antisense oligonucleotides, which are taken-up freely. Experiments focused on simultaneous autophagy modulation and ASO trafficking and activity would provide an understanding of oligonucleotide intracellular fate, trafficking, and delivery beyond the current paradigm of endosome to lysosome.

In this study, we investigated the interdependence of autophagy and ASO localization and activity in tissue culture cells and in mice. We examined autophagic flux following free-uptake and electroporated delivery of ASOs and found that both basal and starvation-induced autophagy are insensitive to ASOs as cargo. To investigate the influence of autophagy on the performance of ASO activity, we evaluated target RNA knockdown during autophagy activation and inhibition. To our surprise, autophagy activation resulted in enhanced knockdown efficiency when ASOs were delivered by free-uptake, while inhibition of the pathway either early in induction or late in maturation resulted in decreased knockdown efficiency. Furthermore, quantitative fluorescence microscopy indicated that the increased activity we observed was clearly associated with enhanced localization of ASOs to autophagosomes. These results were consistent across various cell lines, ASO chemistries and target RNAs. In addition, pharmacological, starvation and ketogenic diet-induced autophagy enhanced ASO activity in mouse liver, providing robust confirmation that this mechanism extends *in vivo*. This work identifies that the autophagosome is an important dynamic compartment that contributes to intracellular ASO trafficking and activity and suggests a novel mechanism to enhance ASO-mediated knockdown efficiency potentially through fasting or autophagy enhancing diets.

MATERIALS AND METHODS

Antibodies, plasmids, siRNAs, ASOs and quantitative real-time PCR (qRT-PCR) primer probe sets, and pharmacokinetic analysis protocols are described in Supplementary Data.

Ethics statement

Ionis is AAALAC accredited and follows the 8th Ed. of the Guide for the Care and Use of Laboratory Animals and the 2013 AVMA guidelines for the euthanasia of animals. All animals in this study were anesthetized with Isoflurane and euthanized via cervical dislocation. The Ionis IACUC-approved protocol is # P-0291-10096. The protocol was approved on 11/27/2018.

Diets

Control (D12450K) and High Fat Ketogenic Diets (D16062902) were purchased from Research Diets Inc. Control diet: protein: 20% kcal; fat: 10% kcal; carbohydrate: 70% kcal; energy density: 3.82 kcal/g. Ketogenic diet: protein: 10% kcal; fat: 89.9% kcal; carbohydrate: 0.1% kcal; energy density: 6.7 kcal/g.

Oligonucleotide synthesis and delivery

ASOs were synthesized at Ionis Pharmaceuticals (Carlsbad, CA, USA) as described previously (24). ASOs were formulated in saline and injected via subcutaneous administration into the animals. In order to monitor reproducibility of the subcutaneous dosing, we used C57BL/6J mice as the control strain for each experiment. Similar levels of *Malat1* inhibition in the livers were observed for experiments with 24-hour timepoints and DMSO or PBS treated mice with respect to chemistry.

Mice

Mice were obtained from The Jackson Laboratory and housed at Ionis Pharmaceuticals (Carlsbad, CA, USA), maintained on a chow diet and entered into studies before they exceeded 8 weeks of age. At the end of each experiment, mice were anesthetized, euthanized by cervical dislocation and blood was collected by cardiac puncture. Spleens, kidneys and livers were harvested and immediately either (i) stored in 4% PFA for 24 h then in 70% ethanol for histological analysis, (ii) snap frozen for protein biochemistry

and (iii) homogenized in Guanidine Isothiocyanate supplemented with 4% BME. Results represent and $n = 4$ mice per treatment condition. As many antisense drugs target liver (4), our main analytical endpoints were hepatic drug accumulation and reduction of Malat1 liver mRNA expression. Despite the hepatic abundance of *Malat1*, its loss of function has been found to be phenotypically silent, with no effect on global gene expression, phosphorylation, splicing factor levels or pre-mRNA splicing events (25,26). ASO tolerability and hepatotoxicity were assessed by measurement of serum aminotransferase (ALT and AST) and spleen weights (Supplementary Figure S10). No post-dose elevations in either serum ALT/AST levels or spleen weights were observed.

Cell lines and reagents

MHT, A431, H4, HeLa, HT1080, HEK293 and human fibroblasts cells were cultured in DMEM supplemented with 10% fetal bovine serum, streptomycin (0.1 mg/ml), and penicillin (100 U/ml) in a 37°C incubator with 5% carbon dioxide, according to the protocols provided by the American Type Culture Collection. Cells were seeded at 50% confluency in 96-well plates or chamber slides 1 day prior to treatments as described. Malat1, SRB1 and control ASOs were added to cells at the indicated concentrations at indicated incubation periods. 5 nmol of ON-TARGETplus pooled-siRNA (Dharmacon, Control, Atg5, and Atg7) was formulated in RNAiMAX plus Opti-MEM (ThermoFisher Scientific) and incubated with cells for 72 h prior to compound and ASO administration. 1 μg of Tfeb cDNA was transiently transfected using Lipofectamine 3000 plus Opti-MEM (ThermoFisher Scientific) and incubated with cells for 48 h prior to compound and ASO administration.

Primary murine hepatocyte isolation

Mouse liver was perfused as previously described (27). Briefly, mice were anesthetized with an intraperitoneal injection of 0.1 ml per 10 g ketamine/xylazine. Inferior vena cava was catheterized and clamped. Liver was perfused with Hank's Balanced Salt Solution (Life Technologies) and mesenteric vessel was cut for drainage. Liver was subsequently perfused with collagenase (Roche). Following the perfusion, liver was removed and gently messaged through sterile nylon mesh. Cells were washed in Williams E (Life Technologies) containing 10% fetal calf serum, (4-(2-hydroxyethyl)-1-piperazineethanesulfonic acid) (HEPES), L-glutamine and antibiotic/antimycotic. Cell separations: Liver perfusions were performed as described above. A portion of the whole liver cell suspension was collected for the whole liver fraction. The fraction was spun at 450 × g, washed with PBS containing 0.5% BSA and 2 mM EDTA (wash buffer), and pelleted. The hepatocyte and non-parenchymal fractions were separated as described previously (27). Whole liver cell suspension was spun at 50 × g. The resulting hepatocyte pellet was washed, spun and run over a 30% percoll (GE Healthcare) gradient. A final wash was performed to remove residual percoll and cells were subsequently pelleted.

RNA preparation and qRT-PCR

Gene expression values were calculated using the comparative delta delta C_t ($-\Delta\Delta C_t$) method and expression against pooled RNA standard curve, using housekeeper gene C_t values and control-treated C_t for normalization as calculated on StepOne Analysis Software v2.3. Total RNA was prepared using an RNeasy mini kit (Qiagen) from cells grown in 96-well plates (*10 000 cells per well). qRT-PCR using TaqMan primer probe sets were performed as described previously (28). In brief, 50 ng total RNA in 5 μl water was mixed with 0.3 μl forward and reverse primers (10 μM of each) and fluorescently labeled probe (3 μM), 0.3 μl RT enzyme mix (Qiagen), 4.4 μl RNase-free water, and 10 μl of 2 · PCR reaction buffer in a 20 μl reaction. Reverse transcription was performed at 48°C for 10 min; 40 cycles of PCR were conducted at 94°C for 20 s and 60°C for 20 s using the StepOne Plus RT-PCR system (Applied Biosystems). Levels of messenger RNA were normalized to the amount of total RNA present in each reaction as determined for duplicate RNA samples using the RiboGreen assay (Life Technologies) or normalized to Cyclophilin A house-keeping gene expression.

Western analysis

Cells were collected using scraper in 1× phosphate buffered saline (PBS) buffer and washed once with 1× PBS. Cell lysate was prepared using radioimmunoprecipitation assay (RIPA) buffer (ThermoFisher) supplemented with 1× Halt Protease Inhibitor Cocktail, EDTA-Free (Life Technologies) and 1× Halt Phosphatase Inhibitor Cocktail (Life Technologies) and cleared by centrifugation at 10 000 × g for 10 min at 4°C. Mouse liver tissues were processed with T-PER Tissue Protein Extraction Reagent (Life Technologies) supplemented with 1× Halt Protease Inhibitor Cocktail, EDTA-Free (Life Technologies) and 1× Halt Phosphatase Inhibitor Cocktail (Life Technologies). Tissue samples were homogenized with Lysing Beads - Matrix D tubes using a FastPrep-24 5G Homogenizer (MP Biomedicals), cleared by centrifugation at 10 000 × g for 10 min at 4°C. Protein concentration was determined by Lowry DC protein assay (Biorad). Proteins (20-40 μg/lane) were separated by 4–12% sodium dodecyl sulphate-polyacrylamide gel electrophoresis (SDS-PAGE), transferred to 0.2/0.4 μm nitrocellulose or 0.2 μm PVDF using standard methods and membranes were blocked in StartingBlock T20 (TBS) Blocking Buffer (Life Technologies). Primary antibodies were diluted in blocking solution and were incubated with membranes at 4°C overnight; HRP (Cell Signaling) or IFR fluorophore-conjugated secondary antibodies (LI-COR) antibodies were diluted in blocking solution and incubated with membranes at room temperature for 1 h. Western blots were detected with the OdysseyCLx imager (LI-COR) or developed using Dura Western Blotting Detection System (Pierce) and exposed to film for images. Protein quantification was performed using Image Studio (LI-COR) analysis software and band densities were normalized to α-tubulin or GAPDH when appropriate.

Immunofluorescent staining

Cells were washed with 1× PBS, fixed with 4% paraformaldehyde for 0.5–1 h at room temperature and permeabilized for 4 min with 0.1% Triton in 1× PBS. After blocking at room temperature for 30 min with block buffer (1 mg/ml bovine serum albumin in 1× PBS), cells were incubated with primary antibodies (1:100–1:300) in block buffer O/N at 4°C then washed three times (5 min each) using wash buffer [0.1% nonyl phenoxypolyethoxylethanol-40 (NP-40) in 1× PBS] and incubated for 1 h with secondary antibody conjugated with fluorophores (1:200). After washing three times, cells were mounted with anti-fade reagent containing DAPI (Life Technologies), and images were acquired using confocal microscope (Leica SP8) and processed using Imaris (BitPlane). Z-stacks were generated from images taken at ∼0.1 μm depth per section, and 3D images were generated using Imaris (BitPlane). For early time staining after ASO incubation (within 2 h), cells were washed three times with acidic buffer (0.1 M acetic acid, 500 mM NaCl) and one time with 1× PBS, to remove cell surface-associated ASOs before fixation. Quantification of co-localization events was performed manually from ∼20 cells, by counting overlapping foci of which images from both channels have clearly defined boundary without saturation. Statistics analysis was performed based on unpaired *t*-test using Prism.

CellLight early endosome (EE) marker was used to visualize early endosomes in MHT cells. MHT cells were treated with CellLight EE and either DMSO or 500 nM AZD8055 for 14 h prior to the addition of Compound No. 851810 at 2 μM by free uptake for 10 h. Confocal images were then obtained and analyzed by counting the total number of early endosomes per cell and the number of early endosomes that colocalized with the antisense oligonucleotide. Results represent the average of 7–8 images. The Premo autophagy tandem sensor RFP-GFP-LC3B was used to visualize autophagy in MHT cells. LysoTracker was used to visualize lysosomes. MHT cells were treated with the Premo sensor and LysoTracker for 2 h, then either DMSO or an autophagy modulator for 14 h. Compound No. 851810 was then added at 2 μM by free uptake for 10 h prior to cell imaging. Confocal images were analyzed by counting the total number of autophagic vesicles per cell and lysosomes per cell as well as the number of autophagic vesicles and lysosomes that colocalized with the antisense oligonucleotide of Compound No. 851810. Results represent the average of 4–6 images.

Confocal imaging. Images for quantitation of puncta were captured with an Lecia SP-8 confocal microscope using a ×60 1.4 numerical aperture (NA) objective (Leica). The images were captured from randomly selected fields of view. Quantitation of surface rendered localization and puncta was performed using the Imaris software from Bitplane/Andor.

Statistics

Data are reported as means ± SEM. Statistical significance was considered when $P < 0.05$. Unpaired Student's *t*-test, One-way or two-way ANOVA with multiple comparisons test have been used to determine significance relative to appropriate control groups. The statistical tests, sample size/replicates, and relative statistical comparisons are mentioned in the figure legends.

RESULTS

ASO administration does not affect basal autophagy

To determine whether ASO administration influences basal autophagy in tissue culture cells, we subjected a mouse hepatocellular SV40 large T-antigen carcinoma (MHT) cell line, which maintains the ability to efficiently take up single stranded oligonucleotides over multiple passages in culture (29), to either free-uptake or electroporation-mediated ASO delivery for a total incubation time of 24 h. We found that delivery of a non-targeting sequence ASO (control ASO) did not alter autophagy as indicated by western blot for LC3B-II/I and p62 protein levels (Figure 1A) as well as immunofluorescent staining of LC3B positive autophagosomes and lysosomes (Figure 1B). Given the reported accumulation of ASOs within the lysosomal compartment, we next examined whether the presence of ASO affects starvation-induced autophagy. MHT cells were treated for 24 h with control ASO (MOE) and then subjected to starvation media to activate autophagy. There was no significant difference between PBS and control ASO-treated cells with respect to autophagy activation as marked by p62 clearance and autophagosome production (increased LC3B II/I Ratio) (Figure 1C), suggesting ASO presence does not affect either basal or induced states of autophagy.

ASOs localize inside of autophagosomes

Since the autophagy pathway intersects with endosomal and lysosomal membrane trafficking at several stages (8), we sought to determine if ASOs are trafficked through autophagy. To answer this question, we co-localized ASOs with autophagosomes in free-uptake competent cell-lines that demonstrate robust ASO target-reduction activity: mouse MHT and human A431 cells. Cell lines were treated with baculovirus expressing the tandem fluorescent-LC3B reporter, which utilizes an acid-sensitive GFP with an acid-insensitive RFP to indicate the transition from autophagosome (neutral pH) to autolysosome (acidic pH). Thus, autophagosomes exhibit RFP/GFP colocalization (yellow), while after fusion with lysosomes, autolysosomes are only shown as red puncta. Cells were treated with either DMSO or AZD8055, a potent catalytic inhibitor of mTORC1 and mTORC2 (30), for 14 h prior to administration of an ALEXA647-conjugated ASO for 10 h. Live-cell imaging revealed clear co-localization of ASO and autophagosomes in both cell lines (Figure 2A). We quantified the number of surface-rendered GFP-LC3B-positive vesicles containing a mean intensity signal ASO and compared this to total autophagosome counts between DMSO- and AZD8055-treated cells. In both cell lines, AZD8055 significantly enhanced autophagy, autophagosome production, and localization of ASO into the autophagosome (Figure 2B; Supplemental Figure S1). Thus, ASOs co-localize within au-

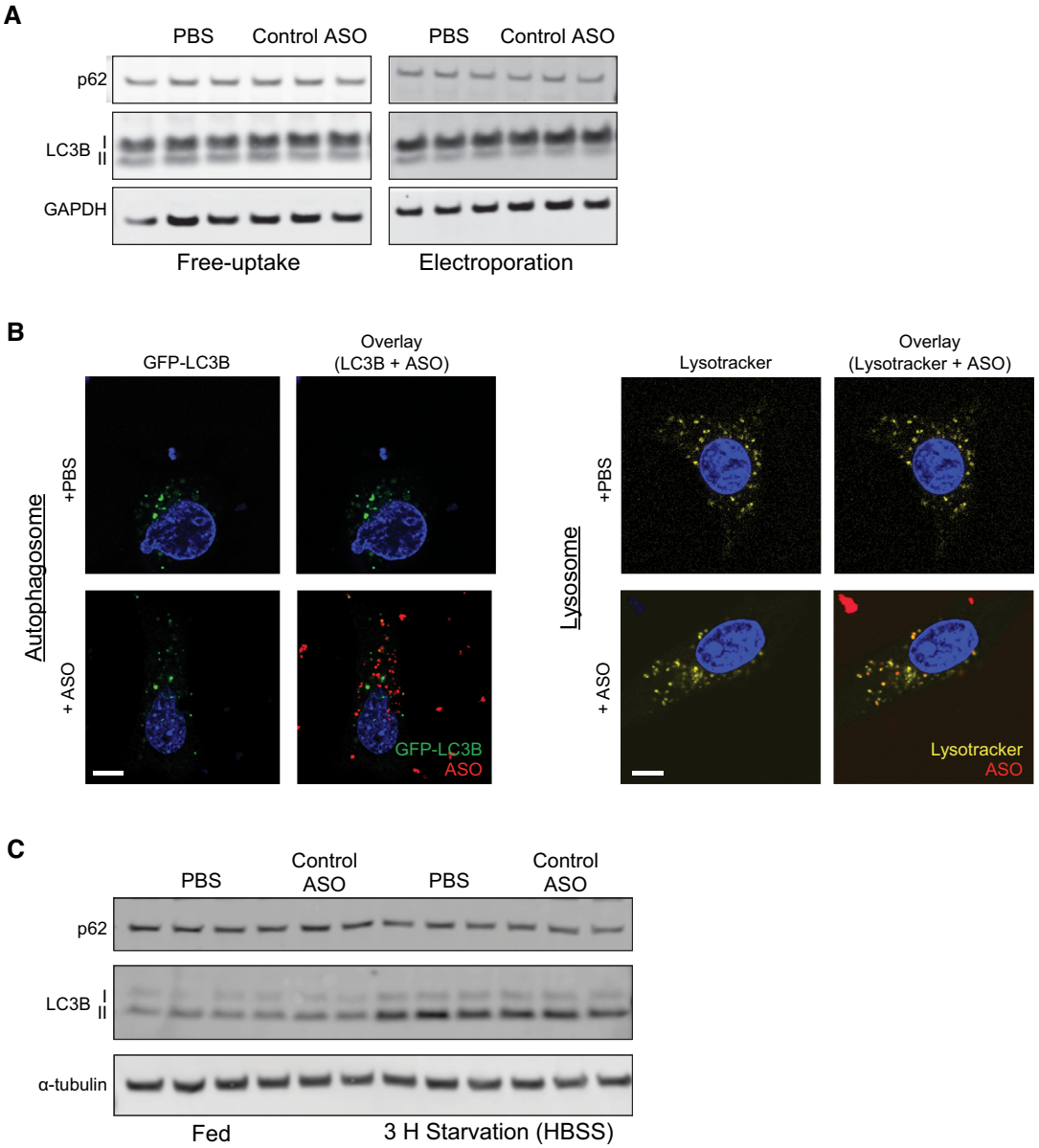

Figure 1. ASO administration does not affect basal or starvation-induced autophagy. (**A**) MHT cells cultured in serum-containing media were incubated or electroporated with either PBS or a non-targeting control ASO (MOE; 5μM) in full culture medium. Twenty four hours post ASO treatment, proteins were collected and analyzed by immunoblotting for LC3 lipidation and p62 degradation with normalization to GAPDH. (**B**) ASO free-uptake has no effect on autophagosome or lysosome vesicle production. MHT cells transiently expressing GFP-LC3B (green) or Lysotracker (yellow) reporters were incubated with PBS or Alx647-labeled ASO (2 μM) (red) for 10 h. Nuclei were stained with Hoechst (blue). Representative images are shown. Scale bar equals 5 μm. (**C**) ASO free-uptake has no effect on starvation-induced autophagy activation. MHT cells cultured in serum-containing media were treated with PBS or non-targeting control ASO (MOE; 5 μM) in full culture medium for 24 h followed by a brief starvation paradigm in HBSS. Three hours post-starvation induction, proteins were collected and analyzed by immunoblotting for LC3 lipidation and p62 degradation with normalization to α-tubulin.

tophagosomes, and activating autophagy with AZD8055 significantly increases this incidence in cells.

Autophagy modulation alters ASO activity *in vitro*

We next sought to determine if ASO activity is regulated by autophagy. To do this, we treated cells with autophagy activators including rapamycin, which allosterically inhibits mTORC1, or AZD8055. In addition, we evaluated the effects of autophagy inhibition using VPS34IN2, which inhibits the PI 3-kinase VPS34 to block autophagosome production and initiation (31), or chloroquine, which impairs autophagosome fusion with lysosomes and lysosomal degradation (32). MHT or A431 cells were treated for 14 h with small molecule autophagy inhibitors or inducers, after which control or Malat1 ASO was administrated via free-uptake for 10 h. ASO administration alone achieved efficient Malat1 reduction compared to control ASO-treated

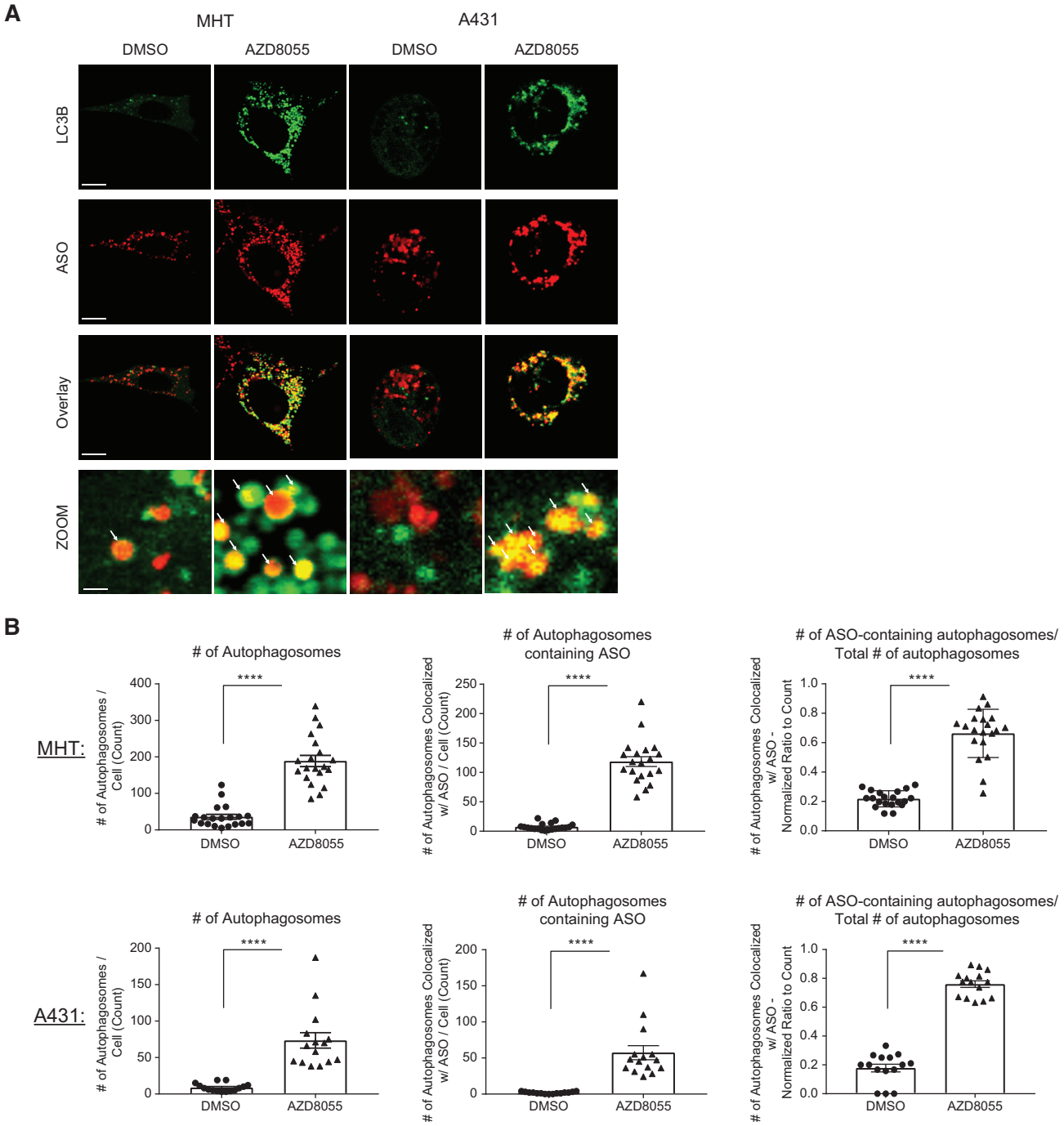

Figure 2. ASOs localize inside of autophagosomes. (**A**) MHT and A431 cells cultured in serum-containing media transiently expressing GFP-LC3B (green) reporter were treated with DMSO or AZD8055 (500 nM) for 14 h followed by incubation with PBS or Alx647-ASO (2 μM; red) for 10 h. Representative images of pre-acidified autophagosomes (GFP-LC3B) and their colocalization with Alx647-labeled ASO are shown. White arrows indicate ASO localization to LC3B autophagosomes. Scale bar equals 10 μm; Zoom panels = 1 μm. (**B**) Relative ASO localization inside of autophagosomes in the presence of activated autophagy. Per-cell quantification of autophagosomes, autophagosomes containing ASO, and autophagosomes containing ASO normalized to total autophagosomes per cell was determined for MHT (top) and A431 (bottom). Data indicate means ± SEM of loci in 20 cells (unpaired *t*-test, $^{****}P < 0.0001$ versus DMSO treated cells).

cells in a dose–responsive manner (Figure 3A for MHT, Figure 3B for A431; DMSO-treated cells). The addition of mTOR-dependent autophagy inducers Rapamycin or AZD8055 significantly enhanced the knockdown efficiency of Malat1 ASO, while autophagy inhibitors VPS34IN2 and Chloroquine suppressed the knockdown efficiency (Figure 3A, B). To evaluate the effect of physiological activation of autophagy on ASO activity, MHT cells were incubated with ASO for 10 h followed by media replacement with HBSS for 10 h to deplete the cells of nutrients. HBSS is commonly used for starvation studies as it lacks essential amino acids and serum. Starvation in MHT cells significantly enhanced ASO activity as measured by reduced Malat1 gene expression (Supplementary Figure S2).

To determine if autophagy-mediated enhancement of ASO activity is mTOR-dependant, we treated MHT cells with trehalose for 48 h followed by free-uptake administration of ASO for 12 h. Trehalose has been suggested to inhibit cellular import of glucose and fructose through SLC2A (GLUT) transporters, producing a starvation-like (low adenosine triphosphate) state in cells that stimulates autophagy and autophagosome production through AMPK and activation of ULK1 (33), which we confirmed in MHT cells (Supplementary Figure S3A). Trehalose significantly enhanced the knockdown efficiency of SRB1 ASO in a dose-dependent manner relative to control ASO-treated cells (Supplementary Figure S3B), similar to Rapamycin and AZD8055, but without affecting mTOR activity (Supplementary Figure S3A). Additionally, the effects of autophagy activation or inhibition on ASO activity appear to be dose-dependent (Supplementary Figure S4A, B).

We next investigated whether autophagy activation modulates ASO concentrations (i) within the cell or (ii) in the extracellular milieu via secretory autophagy (34). We performed hybridization-based bioanalytical ELISA to measure intracellular and extracellular ASO concentrations and found no significant differences in ASO concentrations, either intracellularly or extracellularly in the cell culture media, between cells treated with DMSO, Rapamycin, or AZD8055 (Supplementary Figure S5).

We next asked whether the observed effects on ASO activity through autophagy activation (via AZD8055) or inhibition (via Chloroquine) would be similar if ASO was already present within the cell prior to modulation of autophagy. To address this, MHT cells were seeded for 24 h with SRB1 ASO, followed by media exchange and 24-hour incubation with either DMSO, AZD8055, or Chloroquine. While there were no consistent significant differences between DMSO- and Chloroquine-treated cells (aside from the 0.1 μM ASO treatment group), AZD8055 greatly enhanced ASO activity as marked by a significant decrease in SRB1 gene expression across all ASO concentrations evaluated (Figure 3C) when compared to DMSO and control ASO-treated groups.

We next examined if these effects are dependent on the chemistry of antisense oligonucleotide tested. Cells were treated with next-generation cEt-modified ASOs (Gen 2.5), which demonstrate improved physicochemical, biochemical, and pharmacokinetic properties over previous generations (35). MHT cells were treated using a similar paradigm as described in Figure 3A. Consistent with MOE chemistry ASOs, AZD8055 significantly enhanced cEt-modified Malat1 ASO activity compared to DMSO-treated cells, and Chloroquine significantly inhibited ASO activity as measured by Malat1 gene expression (Figure 3D). We next examined whether GalNac-conjugated ASOs would respond in a similar manner to unconjugated 2′MOE and cEt chemistry ASOs. The addition of AZD8055 significantly enhanced the knockdown efficiency of GalNac-Malat1 ASO in a dose-responsive manner in isolated mouse primary hepatocytes compared to DMSO-treated cells (Figure 3E).

Given the role of autophagy on cell stress response (36), we examined whether any of the administered compounds produce changes in cellular viability or ROS production. Using commercially available cellular ROS/superoxide detection kit and viability fluorescence-based plate assays, we observed no significant changes between ASO-treated and untreated cells in the presence of Rapamycin, AZD8055, VPS34IN2, or Chloroquine compared to DMSO/PBS-treated groups (Supplementary Figure S6A, B). Moreover, these results were also confirmed with various targeting ASOs, with different chemistries, and other cell lines such as H4, HeLa, HT1080 and human fibroblasts with representative results presented (Supplementary Table S1). Target gene expression in all cell lines examined were normalized to either Cyclophilin A house-keeping gene expression or total RNA (Ribogreen), both of which were unaffected by AZD8055, Rapamycin, or Chloroquine treatments (Supplementary Figure S7).

Activation of autophagy enhances ASO localization into autophagosomes but not early endosomes or lysosomes

To determine if enhanced ASO activity upon activation of autophagy is associated with a change in ASO compartment localization and to gain information about temporal events, we performed a kinetic study and dissected the contribution of autophagy and ASO-autophagosome localization to ASO activity. Cells were treated with both high (2000 nM) and low doses (100 nM) of ASOs for short incubation periods of 40 min, 2 h and 4 h and ASO activity was monitored after a medium change and chase duration of 2 h. As expected, treatment with AZD8055 significantly increased total numbers of LC3B-positive autophagosomes consistently across incubation periods compared to DMSO-treated cells, confirming autophagy was activated (Figure 4B, C). For low dose ASO incubation periods and DMSO-treated cells, there was no observed Malat1 mRNA reduction at any of the time points evaluated (Figure 4A). However, in cells with activated autophagy (AZD8055), we observed significant target RNA reduction with 2-hour treatment and further enhancement by 4 h (Figure 4A). With higher doses of administered ASO, DMSO-treated cells showed subtle target RNA knockdown by 2 and 4 h, whereas AZD8055-treated cells demonstrated a significant reduction in gene expression with only 40 min of ASO incubation which was enhanced at longer incubation times (Figure 4A). Interestingly, levels of Malat1 were reduced to the same amount (∼50% of control ASO) in cells treated with either low or high doses of Malat1 ASO during the 4-hour incubation period. Our results show that target mRNA reduction was significantly enhanced when ASOs were administered to cells in an activated autophagic state.

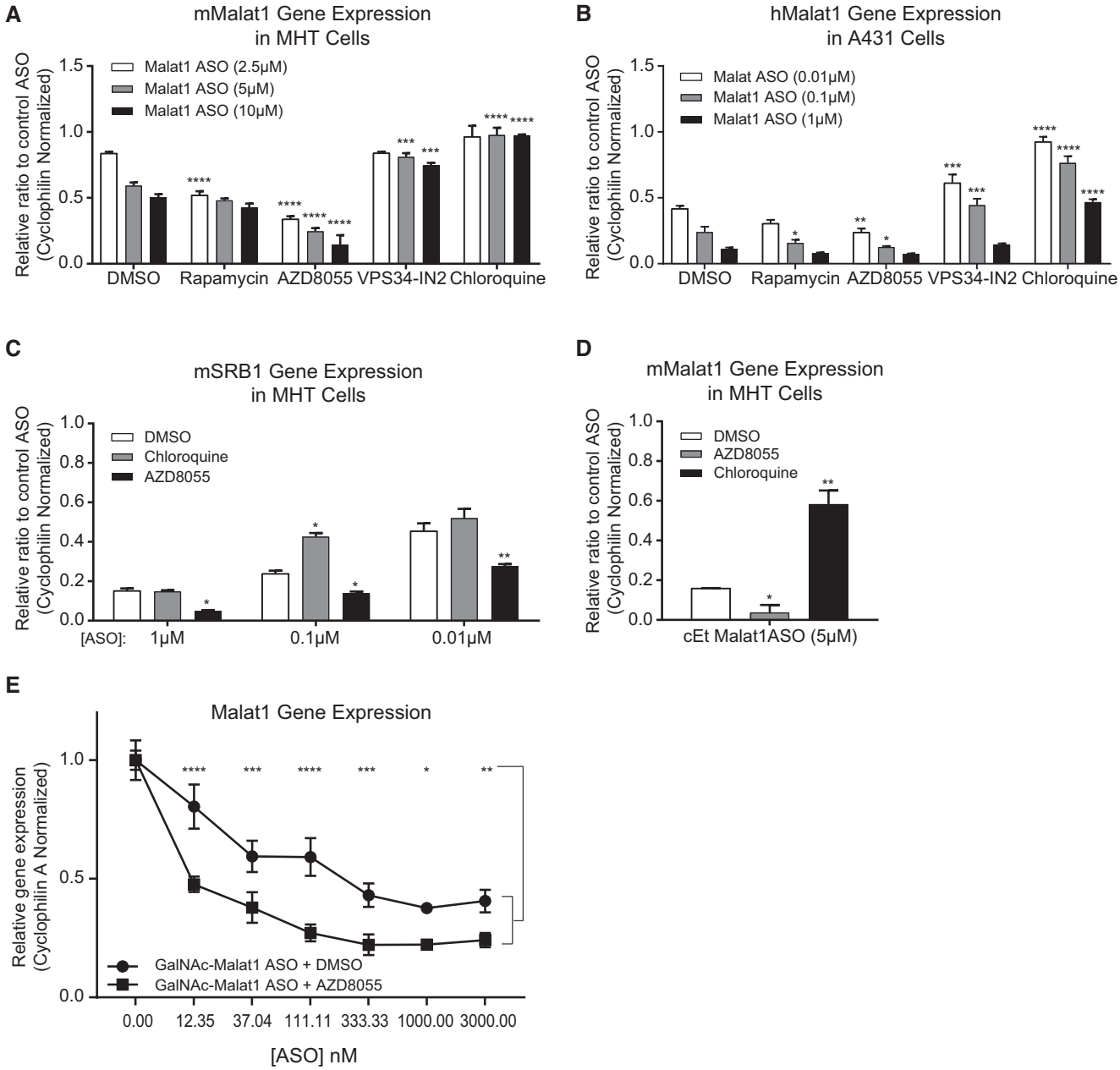

Figure 3. Autophagy modulation via administration of small molecules alters ASO activity. (**A**) MHT and (**B**) A431 cells cultured in serum-containing media were incubated with various concentrations of ASOs (MOE; Control ASO, and either mouse Malat1 ASO for MHT, or human Malat1 ASO for A431; 2.5, 5, 10 μM) for 10 h in the presence of DMSO, Rapamycin (500 nM), AZD8055 (500 nM), VPS34-IN2 (5 μM), or Chloroquine (25 μM), and levels of Malat1 RNA were analyzed by qRT-PCR. (**C**) MHT cells cultured in serum-containing media were incubated with DMSO, AZD8055 (500 nM), or Chloroquine (25 uM) for 24 h in the presence of ASOs (MOE; Control ASO or SRB1 ASO; 0.01, 0.1, 1 μM) for 24 h, and levels of SRB1 RNA were analyzed by qRT-PCR. (**D**) MHT cells cultured in serum-containing media were incubated with ASOs (cEt; Control ASO and Malat1 ASO; 5μM) for 10 h in the presence of DMSO, AZD8055 (500 nM), Chloroquine (25 μM) and levels of Malat1 RNA were analyzed by qRT-PCR. (**E**) Mouse primary hepatocytes were isolated and cultured for 24 h prior to incubatation with ASOs (GalNAc; Control ASO and Malat1 ASO; 0–3000nM) for 10 h in the presence of DMSO, AZD8055 (500 nM), Chloroquine (25 μM) and levels of Malat1 RNA were analyzed by qRT-PCR. All data represent ASO-target gene expressions normalized to Cyclophilin A. Data indicate means ± SEM relative to Control ASO of independent triplicates of one representative experiment out of three repeats (One-way ANOVA, $^{*}P < 0.05$, $^{**}P < 0.01$, $^{***}P < 0.001$, $^{****}P < 0.0001$ versus DMSO-treated cells).

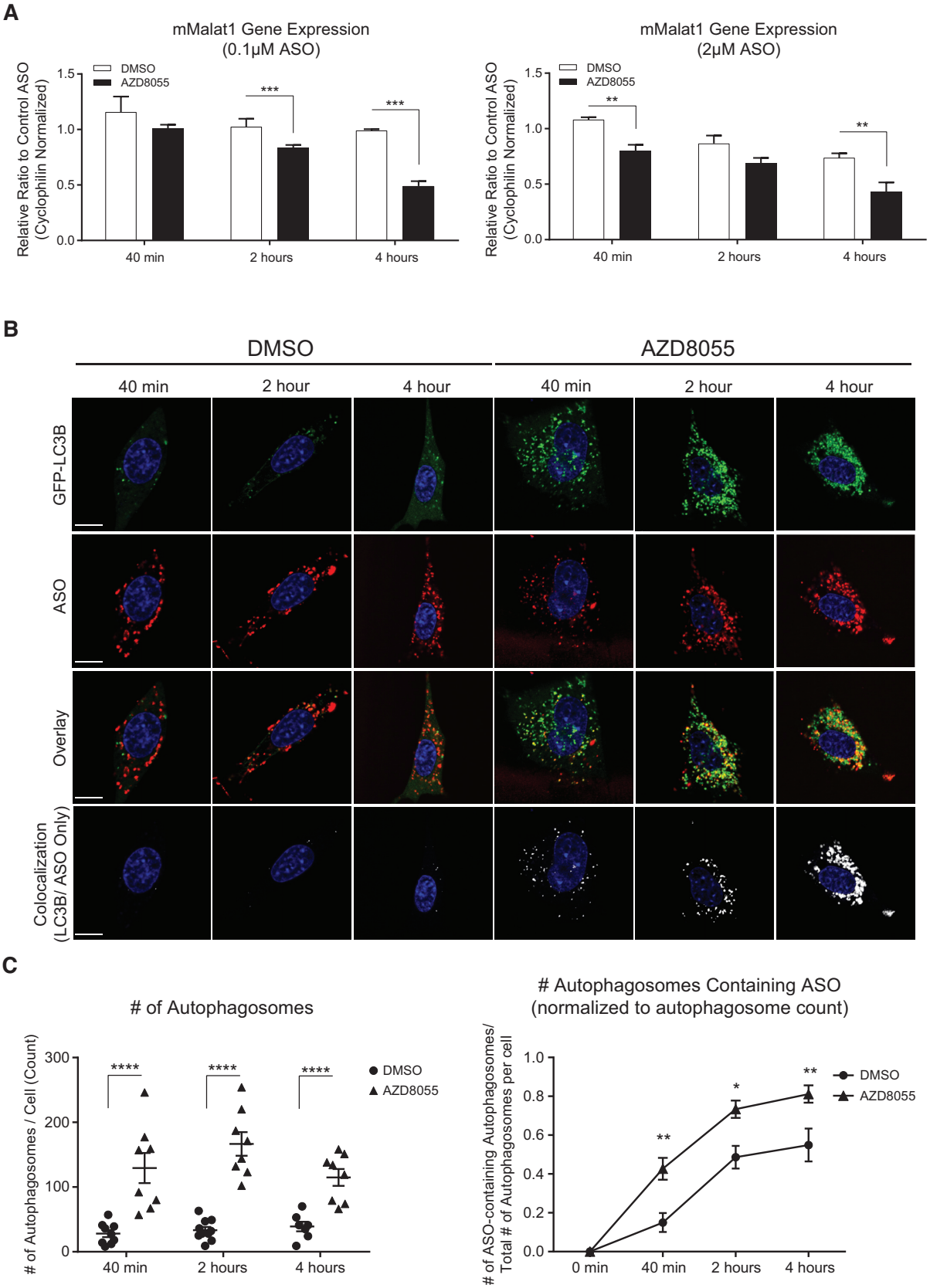
A
mMalat1 Gene Expression
(0.1μM ASO)
Relative Ratio to Control ASO
(Cyclophilin Normalized)
DMSO
AZD8055
1.5
1.0
0.5
0.0
***
***
40 min
2 hours
4 hours
mMalat1 Gene Expression
(2μM ASO)
Relative Ratio to Control ASO
(Cyclophilin Normalized)
DMSO
AZD8055
**
**
40 min
2 hours
4 hours
B
DMSO
AZD8055
40 min
2 hour
4 hour
40 min
2 hour
4 hour
GFP-LC3B
ASO
Overlay
Colocalization
(LC3B/ ASO Only)
C
# of Autophagosomes
# of Autophagosomes / Cell (Count)
300
200
100
0
****
****
****
DMSO
AZD8055
40 min
2 hours
4 hours
Autophagosomes Containing ASO
(normalized to autophagosome count)
# of ASO-containing Autophagosomes/
Total # of Autophagosomes per cell
1.0
0.8
0.6
0.4
0.2
0.0
**
*
**
DMSO
AZD8055
0 min
40 min
2 hours
4 hours

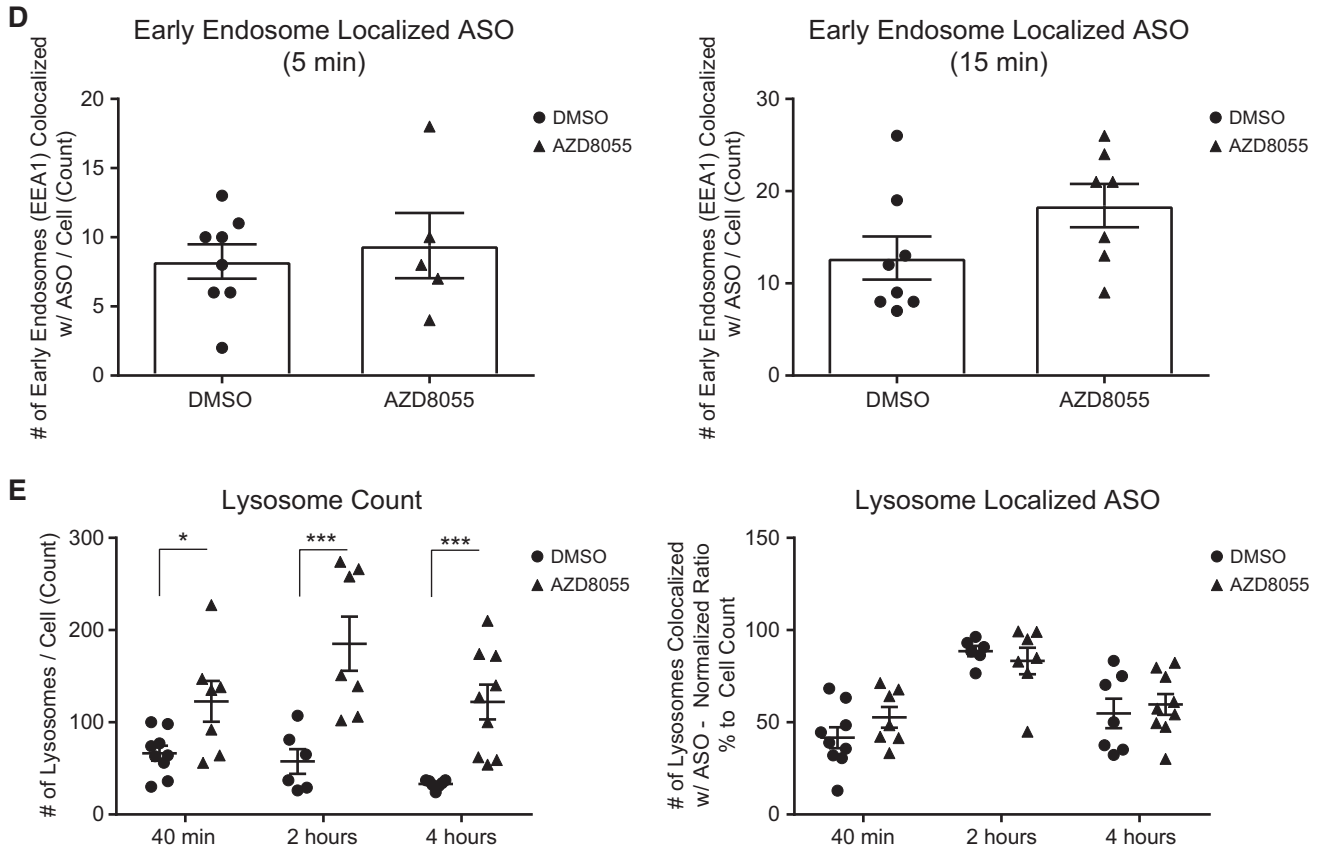

Figure 4. ASO delivery in activated autophagy conditions increases early rate of autophagosome localization but not of localization to early endosomes or lysosomes. (**A**) Kinetic studies on ASO activity for Malat1 RNA reduction. MHT cells cultured in serum-containing media were treated with either DMSO or AZD8055 (500 nM) for 24 h followed by incubation with ASOs (MOE; Malat1 ASO; 0.1 or 2 μM) for 40 min, 2 h or 4 h after which ASOs were removed. Cells were then collected at 2 h after ASO treatment for activity assay and the ASO-target RNA levels were quantified using qRT-PCR. Data indicate means ± SEM of independent triplicates of one representative experiment out of 2 repeats. (**B**) Activated autophagy alters ASO localization into autophagosomes (GFP-LC3B). Representative scans of live MHT cells transiently expressing GFP-LC3B (green), GFP-EEA1, or Lysotracker reporters incubated with Alx647-labeled ASO (2 μM; red), according to the time course described in (A). Images for ASO were merged to show the co-localization (yellow) of ASOs and GFP-LC3B autophagosomes followed by masking to only show ASO localized to GFP-LC3B autophagosomes (white). The nuclei were stained with Hoechst (blue). Scale bar equals 10 μm. (**C**) Quantifications of the total number of autophagosomes and autophagosomes containing ASO normalized to total autophagosomes per cell, (**D**) total number of Early Endosomes and early endosomes containing ASO normalized to total early endosomes per cell, and (**E**) the total number of lysosomes and lysosomes containing ASO normalized to total early endosomes per cell were determined for the indicated time points. Collected images were measured by surface rendering of reporter-labeled vesicles with mean intensity signal of internalized Alx647-labeled ASO with BitPlane Imaris. Scale bar equals 10 μm. Data indicate means ± SEM of results for the average of 5–10 images per condition (unpaired *t*-test, $^{*}P < 0.05$, $^{**}P < 0.01$, $^{***}P < 0.001$, $^{****}P < 0.0001$ versus DMSO treated cells within each time point).

To determine whether enhanced ASO activity is associated with altered intracellular ASO localization following autophagy activation, total number of punctate ASO (presumably vesicle-localized), LC3B-positive autophagosomes, EEA1-postive early endosomes, Lysotracker-positive lysosomes, and respective vesicles containing ASO were quantitated using Bitplane Imaris image analysis software and the related normalized ratios were calculated. Upon activation of autophagy, we observed no significant changes in ASO localization to early endosomes at 5 or 15 min immediately after ASO addition (Figure 4D) or in lysosomes during the chase assay (Figure 4E). Interestingly, however, enhanced autophagy significantly increased the early rate (+69.25% increase) of ASOs localizing to autophagosomes which was maintained across longer free-uptake incubations when compared to DMSO-treated cells (Figure 4B, C).

ASO activity enhancement is independent of TFEB-mediated activation of autophagy

Autophagy can also be regulated by the transcription factor EB (TFEB) which plays a pivotal role in the regulation of lysosomal biogenesis and autophagy through induction of target gene transcription and is itself regulated by mTORC1 (14). To determine if autophagy-mediated enhancement of ASO activity could be directly driven by TFEB-induced autophagosome and lysosome production alone without affecting ULK1 activity, we transiently overexpressed TFEB in MHT cells followed by free-uptake ad-

ministration of ASO for 12 h. We observed significantly increased mRNA expression, protein expression and nuclear translocation of TFEB, along with enhanced autophagy in TFEB-overexpressing cells compared to control transfected cells (Supplementary Figure S8A–C). Additionally, we found subtle and inconsistent inhibition of ASO activity as measured by SRB1 gene expression reduction in TFEB-overexpressing cells compared to the control group (Figure 5A). TFEB overexpression resulted in a significant increase in both autophagosome and lysosome production, accompanied by a significant decrease in the percentage of lysosomes containing ASO (Figure 5C). We found no significant changes in the normalized ASO distribution within autophagosomes across treatment groups (Figure 5D). Additionally, we found that TFEB overexpression resulted in a significant decrease in intracellular ASO concentrations as measured by LLE/SPE and analysed by LC-MS/MS suggesting that activating lysosomal biogenesis through TFEB may mediate degradation of ASO through enhanced lysosomal clearance (Figure 5B). To determine whether autophagy-mediated enhancement of ASO activity driven by mTORC1 inhibition was mediated in part by TFEB activation, we treated MHT cells with mouse TFEB siRNA for 72 h prior to treatment with AZD8055 and SRB1 ASO treatment as previously performed. We found that TFEB reduction significantly enhanced ASO activity relative to control siRNA-treated cells (Figure 5E). Moreover, AZD8055 treatment resulted in a significant enhancement of ASO-mediated gene reduction which was completely unaffected by TFEB knockdown (Figure 5E) suggesting that TFEB is not necessary for mTOR-inhibition mediated enhancement of ASO activity.

Autophagosome formation and autophagy initiation drive the enhancement of ASO activity upon autophagy activation

To determine if autophagy activation affects ASO activity through the initiation of autophagy and production of autophagosomes, we compared ASO activity under autophagy activated conditions driven by AZD8055 with and without co-treatment of a VPS34 inhibitor (SAR405) in a dose-response for 24 h. Cells were subsequently treated with fluorophore-labeled or unlabeled ASOs targeting SRB1 for 10 h to track localization and measure ASO activity, respectively. Consistent with previous reports, SAR405 inhibited AZD8055-driven autophagy activation and autophagosome formation (37) (Figure 6A). Compared to non-SAR405 treated cells, ASO activity as measured by SRB1 RNA reduction was significantly mitigated in a dose-dependent manner with VPS34 inhibition (Figure 6B). Additionally, cells co-treated with SAR405 and AZD8055 exhibited a significantly reduced ratio of autophagosomes containing ASO than cells treated with AZD8055 alone (Figure 6C).

We then examined the contribution of Atg5 and Atg7 to AZD8055-mediated enhancement of ASO activity as these genes are essential for phagophore formation and autophagy (38,39). MHT cells were treated with pooled-siRNAs for 72 h targeting either Atg5 or Atg7, followed by activation of autophagy with AZD8055 and subsequent ASO treatment for 10 h. siRNA-mediated knockdown of Atg5 or Atg7 significantly reduced Atg5 and Atg7 gene expression, respectively (Figure 6D). In MHT cells treated with a control siRNA, AZD8055 significantly enhanced the knockdown efficiency of SRB1 ASO in a dose-dependent manner relative to DMSO-treated cells (Figure 6D). However, upon Atg5 or Atg7 knockdown, AZD8055 had no significant impact on ASO activity relative to DMSO-treated cells indicating that AZD8055-mediated enhancement of ASO activity is dependent on phagophore formation and activation of autophagy (Figure 6D).

Autophagy induction correlates with enhanced ASO activity *in vivo*

Finally, we sought to evaluate the ability of autophagy activation to increase the efficacy of ASO-mediated gene reduction *in vivo.* To activate autophagy in male C57BL/6J mice, we administered 5 mg/kg DMSO, Rapamycin, or AZD8055 every 10–12 h for three total injections, or subjected mice to either a short 16-hour fast or a 5-week ketogenic diet, both of which have been shown to inhibit mTORC1 activity and activate autophagy in mice (40,41). Mice were also given a single 5 mg/kg dose of either PBS, control ASO, or Malat1 MOE ASO (cEt chemistry for Ketogenic Diet) concurrently at the time of initial mTOR inhibitor dosing, food restriction (fasting study), or after 5 weeks on ketogenic diet (Figure 7A). Twenty four hours following initial ASO administrations (or 16 h for fasting study), mice were sacrificed and liver tissue was collected to examine the effects of autophagy induction on ASO activity. In mice treated with either AZD8055 (Figure 7B), Rapamycin (Figure 7C), a short fasting paradigm (Figure 7D), or 5-week ketogenic diet (Figure 7E), autophagy was significantly activated in livers as indicated by suppression of mTOR kinase activity (pS6/S6 levels) and increased LC3B II/I ratio. Consistent with our *in vitro* data, activation of autophagy significantly enhanced ASO activity as demonstrated by greater Malat1 gene expression reduction in the livers of mice treated with AZD8055, Rapamycin, 16-hour fasting regimen, and ketogenic diet (Figure 7F). Autophagy activation did not result in a significant or consistent change in liver ASO concentrations as measured by LLE/SPE and analysed by LC–MS/MS (Supplementary Figure S9A–D). Additionally, no significant changes in plasma ALT/AST levels, organ, or animal weights were observed in any of the treatment groups (Supplementary Figure S10A–D). Finally, we sought to evaluate the short and long-term kinetics of the *in vivo* effects of ketogenic diet-induced autophagy on ASO activity. Male C57BL/6J mice were subjected to a 5-week ketogenic diet prior to administration of a single bolus 5 mg/kg dose of either PBS, control ASO, or Malat cEt ASO for either 24, 48 or 72 h (short term) or 1, 2 or 3 weeks prior to tissue collection. Mice fed a ketogenic diet exhibited significantly enhanced ASO activity across all three short-term time points relative to normal diet-fed mice (Figure 8A). Interestingly, we found that ASO-mediated gene reduction continued to increase from ∼81% at 24 h to ∼90% target reduction at 72 h following a single ASO injection in mice fed a ketogenic diet versus mice fed a normal diet in which ASO activity plateaued at ∼70% target reduction (Figure 8A). Upon examining long term ASO activity, we

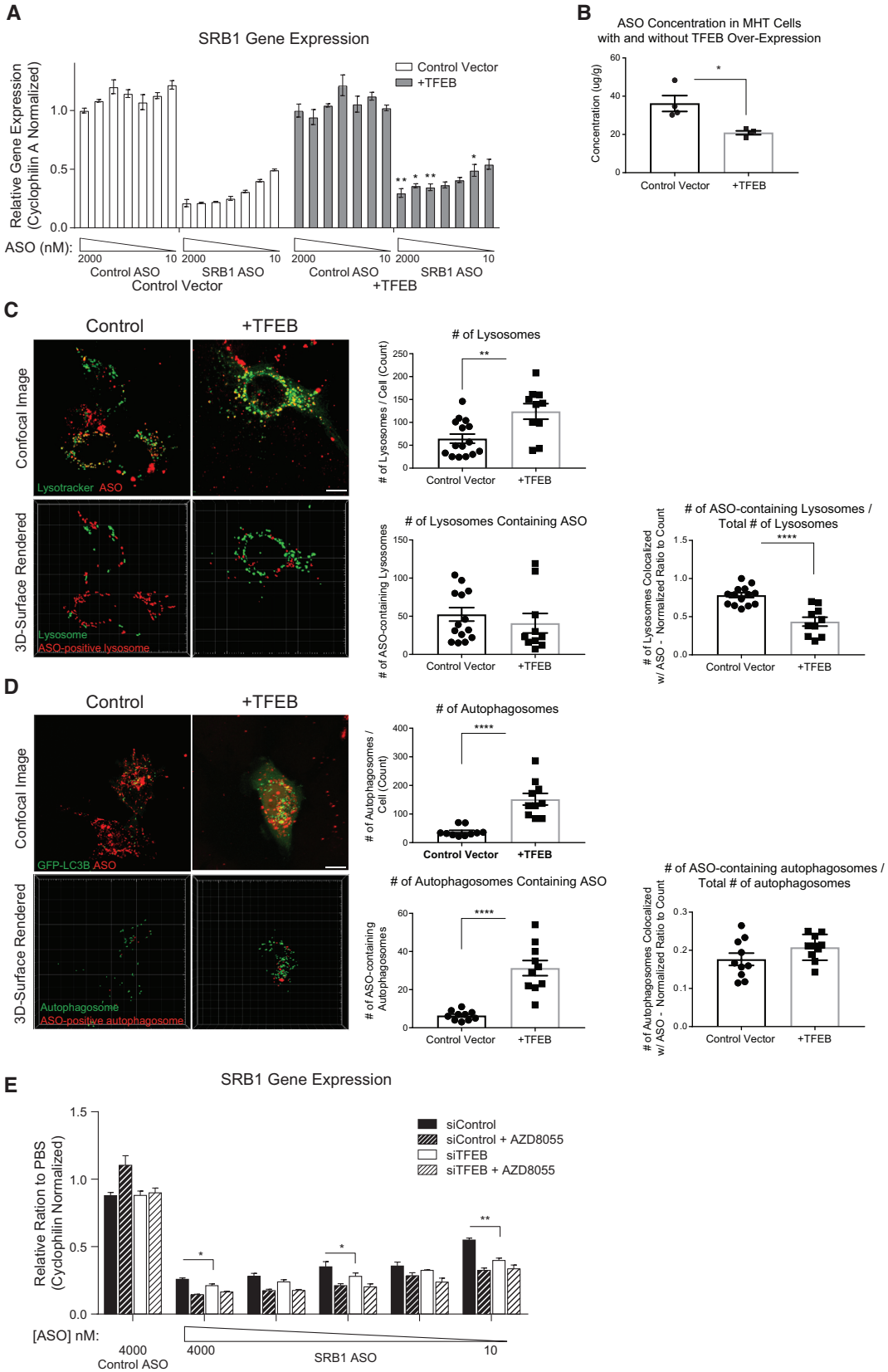

Figure 5. TFEB-mediated activation of autophagy has inhibitory effects on ASO activity in MHT cells. (**A**) MHT cells cultured in serum-containing media were lipofectamine transfected with either control pcDNA or TFEB plasmids (1 μg). Control pcDNA (white bars) or TFEB overexpressing (gray bars) MHT cells were incubated with either Control or SRB1 ASO (MOE; 10–2000 nM) at various doses for 12 h and SRB1 RNA levels were determined using

found that mice fed a ketogenic diet consistently maintained a significant enhancement in activity (∼20–30%) versus normal diet at 1, 2 and 3 weeks post-single ASO administration (Figure 8B). These findings suggest that administration of ASOs into an activated autophagic state driven by ketosis does not result in saturated activity at 24 h but rather continual enhancement of activity over a short-term period (∼72 h) followed by maintained enhancement over time following a single ASO dose (3 weeks). Given previously published findings of mTOR inhibition and autophagy activation in muscle tissue following ketogenic diet administration (42), we examined whether ASO activity was also enhanced in muscle similar to liver, following single-dose administered ASO. We found that mice treated with ketogenic diet had significantly enhanced ASO activity, as measured by Malat1 gene expression in muscle tissue, 1-week following single-dose ASO administration (Figure 8C).

DISCUSSION

It has been suggested that productive ASO release occurs primarily from the LE and an unknown cellular compartment (28,43). In this study, we identified that autophagosomes, which are known to interact with LEs, contribute significantly to ASO trafficking and activity under physiologically-relevant ASO uptake and delivery mechanisms in both cultured cells and animal models. When nutrients are non-limiting and/or mTORC1 is active, the default contribution of autophagy to ASO activity is relatively low. However, activation of the autophagy pathway prior to or following free-uptake of ASOs significantly enhances colocalization of ASOs with autophagosomes. Further, there is a clear correlation between ASO-autophagosome colocalization and enhanced target RNA knockdown suggesting that this compartment may contribute to productive activity and/or release of ASOs.

Although the properties of oligonucleotide trafficking and delivery have been extensively studied and optimized for many years, the precise mechanisms by which endolysosomal escape occurs are not fully understood. Autophagy is a key pathway that bridges endosome-to-lysosome trafficking, but its role in ASO biology has been understudied. A better understanding of the interactions between autophagy and intracellular oligonucleotide trafficking is critical to uncover mechanisms of ASO escape from non-productive compartments. The main features of autophagy are the biogenesis and maturation of autophagosomes, processing, and delivery of certain cargo to the lysosome, suggesting that autophagy may somehow contribute to intracellular ASO delivery and trafficking through its interactions with the endo-lysosomal cascade. Interestingly, the effects we observed upon modulating autophagy both *in vitro* and *in vivo* on ASO activity are dose-responsive and depend on the level of autophagy activation achieved. AZD8055 administration consistently showed the most potent activation of autophagy and autophagosome production, followed by Rapamycin, and then fasting or nutrient deprivation. The level of enhancement of ASO activity with these treatment paradigms followed similar trends. Additionally, ketogenic diet groups demonstrated a 57% enhancement of cEt ASO activity compared to control diet-fed mice which was marked by a robust suppression of mTORC1 activity and activation of autophagy. These effects may be due to the inherent mechanisms by which autophagy and autophagosome biogenesis is initiated. Recent reports have shown that acute starvation-mediated activation of autophagy initially involves endosomal microautophagy and that only after prolonged nutrient deprivation, does macroautophagy turn on (44,45). During this acute selective autophagy, many autophagosomal factors become substrates for endolysosomes. This delay in canonical autophagosome biogenesis during the early stages of starvation-induced autophagy when compared to small molecule-mediated or ketogenic diet-mediated mTOR inhibition may explain the weaker effect observed with fasting compared to the other treatment groups. Accordingly, a longer fasting regimen may provide sufficient time for macroautophagy to commence and have greater impact on ASO activity. These observations suggest that ASO activity may correlate, beyond a certain threshold, with the level of autophagy activation and the rate of autophagosome biogenesis. Additionally, our findings that ASO activity can be continuously enhanced in mice treated with a ketogenic diet over time suggests that this effect may be propagating rather than saturating.

A critical question stemming from these studies is how is ASO localization within autophagosomes resulting in enhanced ASO activity. Similar to endosomes, the primary termination point for autophagosomes is fusion with the lysosome. Because of this, it is surprising that ASO local-

←

qRT-PCR. Sample gene expressions were normalized to Cyclophilin A. Data indicate means ± SEM relative to Control ASO of independent triplicates of one representative experiment out of three repeats (two-way ANOVA w/ Sidak's Multiple Comparisons, $^{*}P < 0.05$, $^{**}P < 0.01$ versus control pcDNA treated cells at each ASO dose). (**B**) MHT cells cultured in serum-containing media were lipofectamine transfected with either control pcDNA or TFEB plasmids (1 μg) followed by free-uptake incubation with 2 μM of Control ASO (MOE) for 24 h. Following ASO incubation, cell concentrations (μg/g) of Control ASO was examined using LCMS/MS. Values are presented as mean ± standard deviation (One-way ANOVA w/ Tukey's multiple comparisons versus DMSO-treated cells; $n = 4$ per group). (C, D) MHT cells transiently expressing (**C**) Lysotracker or (**D**) GFP-LC3B (green) reporters were transiently transfected with either control pcDNA or mTFEB (1 μg). Following 48 h after transfection, cells were incubated with Alx647-ASO (2 μM; red) for 12 h and imaged. Representative images of Alx647-labeled ASO localization, colocalization and presence within surface rendered autophagosomes (GFP-LC3B) or lysosomes (Lysotracker) are shown. Collected images were measured by surface rendering of reporter-labeled vesicles with mean intensity signal of internalized Alx647-labeled ASO with BitPlane Imaris. Total number of lysosomes/autophagosomes, lysosomes/autophagosomes containing ASO and lysosomes/autophagosomes containing ASO normalized to total lysosomes/autophagosomes per cell was determined. Scale bar equals 10 μm. Data indicate means ± SEM of results for the average of 10–15 images per condition (unpaired *t*-test, $^{**}P < 0.01$, $^{****}P < 0.0001$ versus Control pcDNA-treated cells). (**E**) MHT cells were transiently transfected with pooled-control siRNA (black bars), or TFEB siRNA (white bars) for 72 h followed by treatment with DMSO (no stripes) or AZD8055 (stripes) for 24 h, and subsequent incubation with various doses of control or SRB1 ASO (MOE; 10–4000 nM) for 12 h. SRB1 RNA levels were determined using qRT-PCR and normalized to Cyclophilin A. Data indicate means ± SEM relative to Control ASO of independent triplicates of one representative experiment out of two repeats (one-way ANOVA, $^{****}P < 0.0001$ versus control siRNA-treated cells).

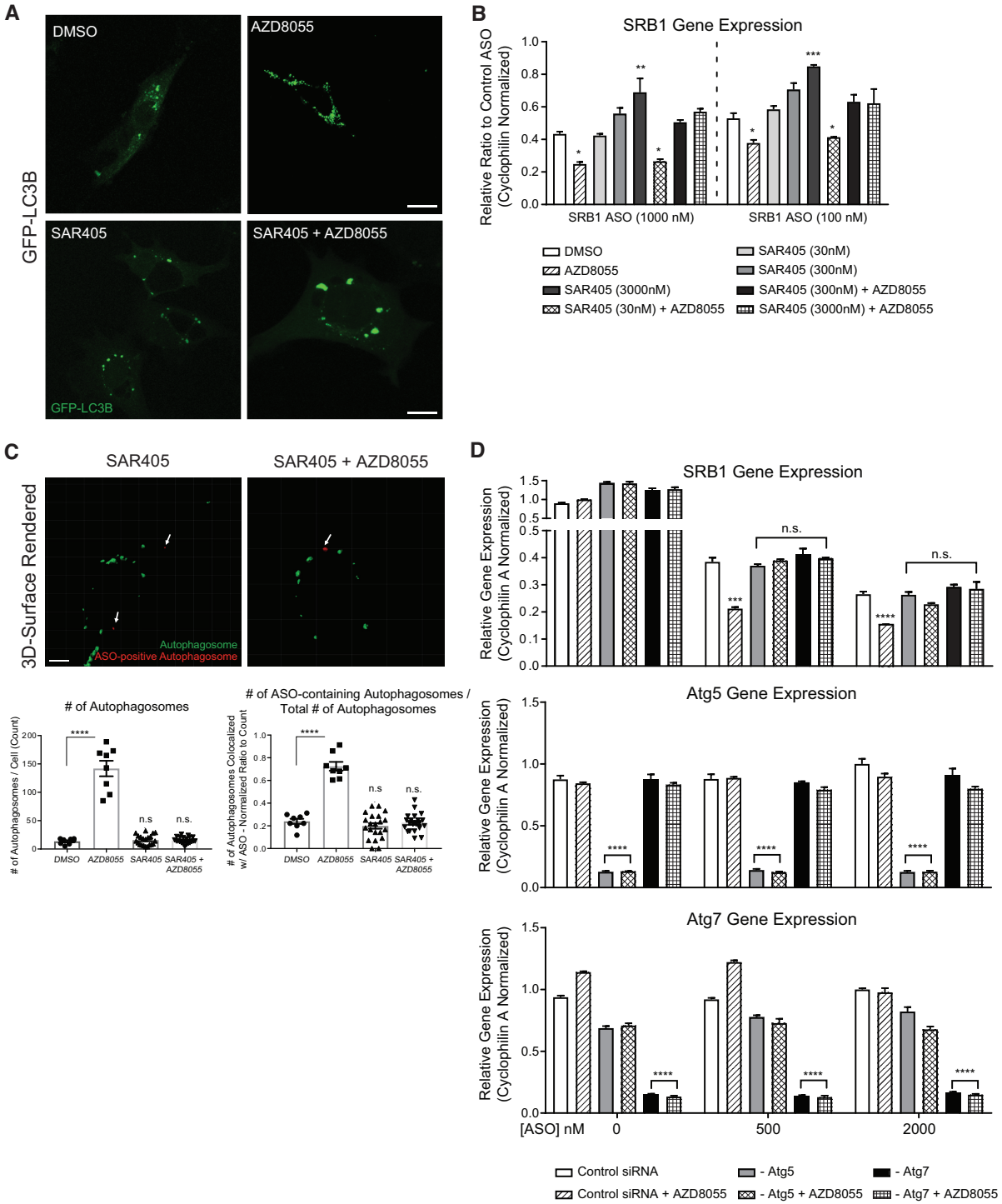

Figure 6. Inhibition or reduction of factors involved in autophagy initiation and autophagosome formation mitigates AZD8055-driven enhancement of ASO activity. (**A**) Representative images of autophagosome production (GFP-LC3) in MHT cells cultured in serum-containing media transiently expressing GFP-LC3B (green) reporter treated with either DMSO, AZD8055 (500 nM), SAR405 (3000 nM), or AZD8055 and SAR405 (500 nM; 3000 nM, respectively). Scale bar equals 10 μm. (**B**) MHT cells cultured in serum-containing media were incubated with various concentrations of SRB1 ASO (MOE; 100 and 1000 nM) for 10 h in the presence of DMSO, AZD8055 (500 nM), SAR405 (30, 300, or 3000 nM), or AZD8055 and SAR405 (500 nM; 30, 300 or 3000 nM, respectively) and levels of SRB1 RNA were analyzed by qRT-PCR followed by normalization to Cyclophilin A expression. Data indicate means ± SEM relative to Control ASO of independent triplicates of one representative experiment out of 2 repeats. (One-way ANOVA, $^{*}P < 0.05$, $^{**}P < 0.01$, $^{***}P < 0.001$ versus DMSO-treated cells within each ASO dose group). (**C**) MHT cells cultured in serum-containing media transiently expressing GFP-LC3B (green) reporter were treated with either SAR405 (3000 nM) or AZD8055 and SAR405 (500 nM; 3000 nM, respectively). Following 24 h treatment, cells were incubated with Alx647-labeled ASO (2 μM; red) for 12 h and imaged. Representative images of Alx647-labeled ASO localization, colocalization and presence within surface rendered autophagosomes (GFP-LC3B) are shown. Collected images were measured by surface rendering of reporter-labeled vesicles with mean intensity signal of internalized Alx647-labeled ASO with BitPlane Imaris. Total number of autophagosomes and autophagosomes con-

ization within autophagosomes is correlated with higher ASO activity, as endosomal and lysosomal escape has been suggested to be the rate-limiting step in antisense activity. A possible explanation for these results may lie within the autophagosome formation process itself. Autophagosomes appear de novo and while the exact origins and mechanisms of their formation is still under investigation, it has been suggested that a potential frequent and proximal membrane source for new forming phagophores upon autophagy induction is the ER and Golgi (46). Interestingly, ASOs have been shown to localize in various perinuclear structures and Golgi-58K-related cytoplasmic vesicles upon free-uptake (5). It is possible that, upon initiation of autophagosome production, various membrane pools containing ASO are shuttled to the forming phagophore and subsequently taken up. It is potentially at this point during autophagosome formation, just prior to phagophore closure and completion, that ASOs may potentially leak and escape delivery to the lysosome.

Another possible membrane and potential source of ASOs for forming autophagosomes is the endo-lysosomal network itself. Given that autophagosomes interact at several nodes within the endo-lysosomal system, one question is whether autophagy activation is shuttling ASO away from the late endosome (LE) compartment. While we attempted to examine this effect concurrently with our investigation of early endosomes and lysosomes, we were unable to examine potential ASO localization shifts to and from the LE. This was primarily due to the observed and reported involvement of canonical LE proteins and selection markers (e.g. Rab5, Rab7, CD63, LBPA) in the normal progression and initiation of autophagy (47–51). Shortly after autophagosomes form, they acquire proteins and enzymes that are normally found in multivesicular bodies, LEs, and lysosomes (52,53), which supports a model in which diverse membrane components are delivered by vesicle fusion to the forming autophagosome membrane. For example, we find that almost immediately upon activation of autophagy, Rab7 colocalizes with LC3B-positive autophagosomes, making it challenging to distinguish LE vesicle pools from newly formed autophagosomes (Supplementary Figure S11). This may provide some evidence that the autophagosome-localized ASO is derived from LE pools. Indeed, it has been suggested that endosomes, in addition to other compartments such as recycling endosomes, trans-Golgi vesicles, and endoplasmic reticulum, may serve as possible sources for the lipid bilayers of forming autophagosomes (54–56). Interestingly, we did not observe a significant change in ASO distribution to the autophagosome or enhancement of ASO activity upon autophagy activation through TFEB overexpression. One explanation for this may be that the lipid and membrane pools by which autophagosome biogenesis occurs are different between mTORC1-direct versus TFEB-mediated induction. While it is important to note that TFEB does have extensive interplay with regards to mTOR signaling (15), little is known about the differences in autophagosome biogenesis between activation of the two. Additionally, we observed that TFEB-overexpressing cells have a significantly decreased ratio of total lysosomes that contain ASO along with overall decreased concentration of ASO within the cell, suggesting there may be enhanced clearance of lysosomal cargo. Interestingly, knockdown of TFEB resulted in slightly enhanced ASO activity independent of mTOR inhibition further suggesting that lysosomal biogenesis and sequestration into this non-productive sink may contribute to inactivity of ASOs. Moreover, alterations in vesicle trafficking facilitated by simultaneous lysosome and autophagosome biogenesis may also contribute to the lack of an effect on ASO activity with TFEB activation. Presumably, certain lipid sources may contain pools of accumulated ASO, which may consequently shuttle to forming phagophores upon autophagy induction and thus shift oligonucleotide localization from a non-productive to potentially productive compartment. A better understanding with regards to phagophore formation, lysosomal contributions, and vesicle dynamics will be needed to tease apart these mechanisms in the future.

Autophagosomes are believed to form randomly throughout the cytoplasm, are trafficked along microtubules toward and away from the nucleus, and ultimately fuse with lysosomes near the perinuclear region of the cell (47,57). Various live-imaging studies have shown that mature autophagosomes move along microtubule tracks toward lysosomes and that the localization of lysosomes determines the rate of autophagosomal fusion. Increasing the perinuclear localization of lysosomes by depletion of certain kinesin factors such as KIF1B-β and KIF2A leads to increased autophagosomal fusion, whereas dispersion of lysosomes to the periphery by overexpressing these motors, decreases fusion rates (58). It is possible that by significantly enhancing the number of inputs to the lysosome through simultaneous endocytic and autophagic activity that the rate of autolysosomal fusion is slowed. In addition to this process is the balance between bulk conversion by compartment fusion with the lysosome versus conversion of an autophagosome to an endosome-like compartment mediated by vesicle trafficking and fusion. The former would be an efficient and rapid single-fusion event, whereas the latter would be presumably a slower process, but would allow a stepwise remodeling of the maturing autophagosome. In both cases, the unresolved issue is how recognition between fusion partners is established and how the rate of these fusions impacts trafficking and localization of internalized cargo. Further these intermediate-vesicles may

←

taining ASO normalized to total autophagosomes per cell was determined. Data indicate means ± SEM of results for the average of 8 (DMSO, AZD8055) and 21 (SAR405, SAR405/AZD8055) images per condition (One-way ANOVA, $^{****}P < 0.0001$ versus DMSO-treated cells). (**D**) MHT cells cultured in serum-containing media were transiently transfected with pooled-control siRNA (white bars), Atg5 siRNA (gray bars), or Atg7 siRNA (black bars) for 72 h followed by treatment with DMSO or AZD8055 for 24 h, and subsequent incubation with various doses of control or SRB1 ASO (MOE; 500 or 2000 nM) for 12 h. SRB1, Atg5 and Atg7 RNA levels were determined using qRT-PCR and normalized to Cyclophilin A. Data indicate means ± SEM relative to Control ASO of independent triplicates of one representative experiment out of two repeats (one-way ANOVA, $^{****}P < 0.0001$ versus control pcDNA-treated cells).

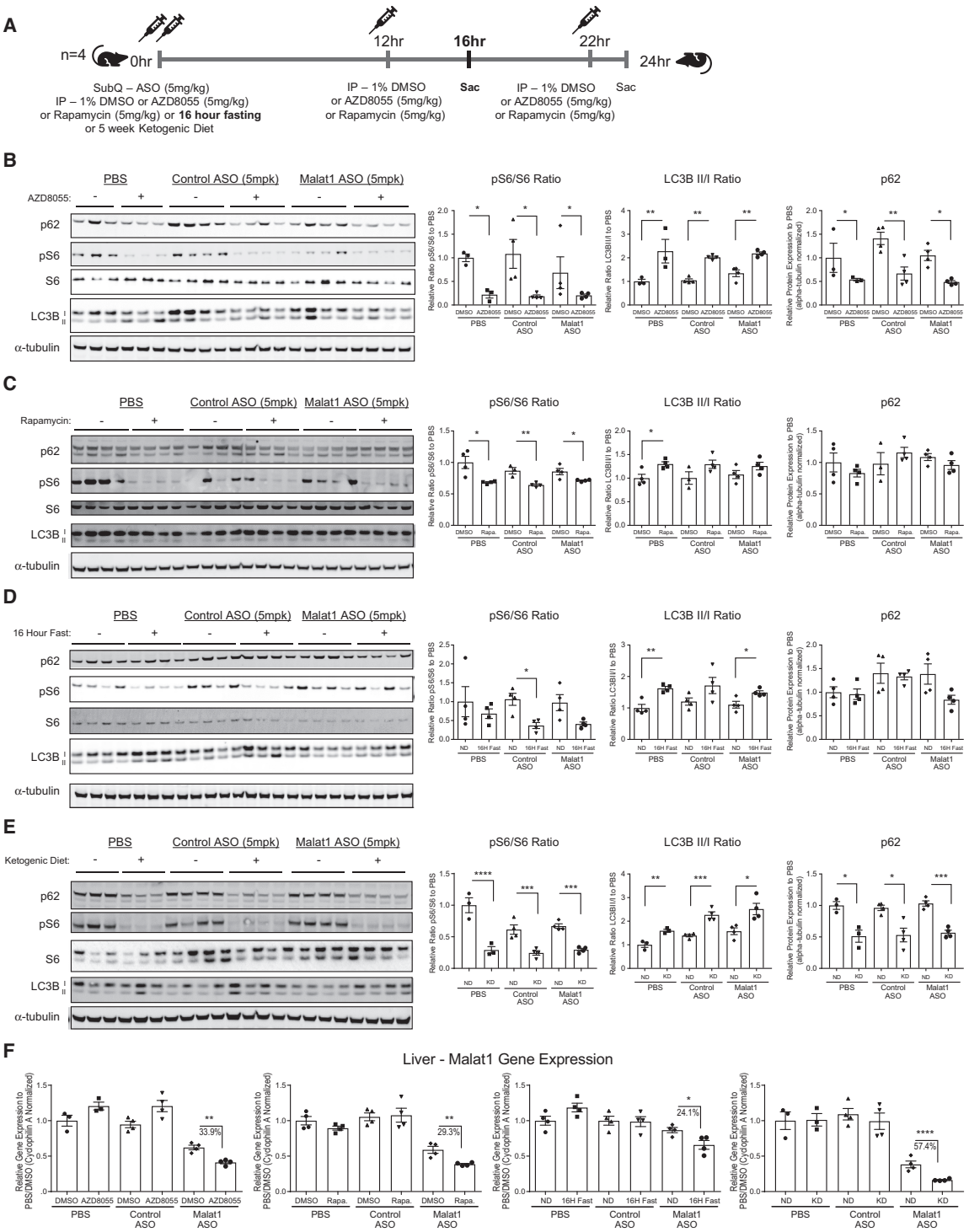

Figure 7. Autophagy induction in liver enhances ASO activity in C57/BL6 mice. (**A**) 8-week-old, male, C57BL/6J mice were administered intraparietal injections of DMSO, AZD8055 (5 mg kg^{-1}), or Rapamycin (5 mg kg^{-1}), had food withdrawn, or were fed a ketogenic diet for 5-weeks immediately prior to a single subcutaneous injection of PBS, Control ASO or Malat1 ASO (5 mg kg^{-1}; MOE for Rapamycin, AZD8055, and fasting; cEt for Ketogenic diet). Autophagy small molecule administration, fasting paradigm, or ketogenic diet were performed as described in (A) to maintain activated autophagy and mice were sacrificed 24 h after ASO administration for analysis (except for in fasting paradigm, where mice were sacrificed following 16 h fasting and ASO administration). (B–E) Liver tissue was processed and proteins were collected and analyzed by immunoblotting for mTOR activity (pS6/S6 ratio), LC3 lipidation, and p62 degradation with normalization to α-tubulin for animals treated with AZD8055 (**B**), Rapamycin (**C**), a 16 h fasting paradigm (**D**), or 5-week Ketogenic diet administration (**E**). Data indicate means ± SEM relative to PBS-treated controls and normalized to α-tubulin when indicated, with independent quadruplicates of one representative experiment. (**F**) Liver tissue was processed and RNA was isolated. Malat1 RNA was analyzed by qRT-PCR and gene expression normalized to Cyclophilin A for AZD8055, Rapamycin, 16 h fasting, or 5-week Ketogenic diet groups. Data indicate sample means ± SEM relative to PBS-treated mice of independent quadruplicates of one representative experiment (One-way ANOVA w/ Tukey's multiple comparisons; $^{*}P < 0.05$, $^{**}P < 0.01$, $^{***}P < 0.001$ versus PBS- or ND-treated mice). ND = Normal diet, KD = Ketogenic diet.

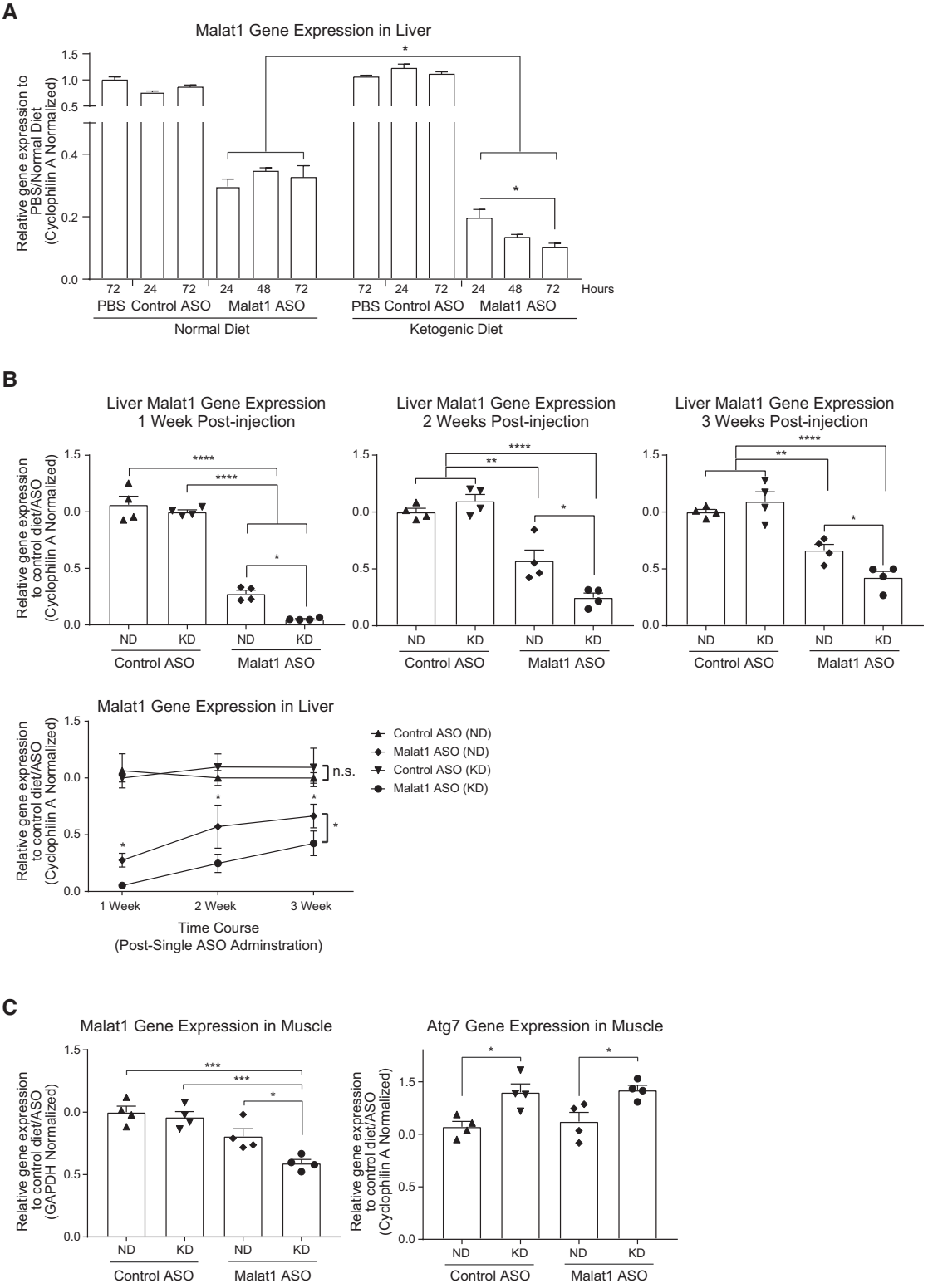

Figure 8. Autophagy induction in liver and muscle with ketogenic diet administration enhances ASO activity in C57/BL6 mice. 8-week-old, male, C57BL/6J mice were fed a ketogenic diet for 5-weeks to maintain activated autophagy immediately prior to a single subcutaneous injection of PBS ($n = 4$/time point), Control ASO ($n = 4$/time point) or Malat1 ASO ($n = 4$/time point) (5 mg kg^{-1}; cEt). Mice were sacrificed either 24, 48, 72 h (**A**) or 1, 2, 3 weeks (**B**) after ASO administration for analysis. (A, B) Liver tissue was processed and RNA was isolated. Malat1 RNA was analyzed by qRT-PCR and gene expression normalized to Cyclophilin A. (**C**) Muscle tissue was processed and RNA was isolated. Malat1 RNA was analyzed by qRT-PCR and gene expression normalized to GAPDH. Data indicate sample means ± SEM relative to Control Diet/Control ASO-treated mice of independent quadruplicates of one representative experiment (one-way ANOVA with Tukey's multiple comparisons; $^{*}P < 0.05$, $^{**}P < 0.01$, $^{***}P < 0.001$, $^{****}P < 0.0001$ versus ND-treated mice). ND = normal diet, KD = Ketogenic diet.

perhaps be more inherently leaky should they persist due to a deficiency of dense and mature lysosomes with which to fuse. In fact, it has been shown that autophagosomes dock onto lysosomes, independent of lysosomal acidification and that two kinds of fusion events can potentially occur: complete fusions which generate a hybrid organelle such as an amphisome, or more often kiss-and-run interactions where there is partial transfer of some content while still maintaining two separate vesicles (57). The rates of these events are thought to depend largely on vesicle numbers and flux and thus, may potentially contribute to oligonucleotide trafficking and escape. Though several molecular components have been identified to support these processes, there are still many unanswered questions that await an understanding of the full molecular mechanism and dynamics of how autophagosome biogenesis occurs and how the autophagy pathway interacts with other trafficking networks.

The pharmacological effects of ASOs are highly varied such that even upon comparable levels of uptake, activities of ASOs can be rather different between cell types (59). On a broader scale, given the reported wide range of basal autophagy and flux across cell lines, tissues, and systems (60–62), it is possible that the differing rates of forming autophagosomes and subsequent interactions with the endo-lysosomal network may contribute to the differences in ASO activity observed. Future studies will be needed to tease apart the contributions and crosstalk between vesicle trafficking and autophagy, and ASO uptake and activity across cell types where these differences are observed. Our findings that metabolic cellular changes induced by serum starvation in cells or fasting and ketosis in mice can contribute to progressive enhancement of ASO activity may provide a rationale for evaluating the interplay between basal autophagy state, autophagy flux changes in response to cell perturbation, and respective ASO therapeutic activities. Given the reported engagement of mTOR inhibition and autophagy activation following ketogenic diet administration in the CNS tissues such as hippocampus (63), one would predict similar findings of enhanced ASO activity to that demonstrated in the liver and muscle, in brain tissue following ICV-administered compounds. Additional studies will be needed to investigate this hypothesis.

In the present study, we have shown that altered autophagy levels both *in vitro* and *in vivo* can influence ASO knockdown efficiency and localization. Our studies suggest a novel mechanism to enhance ASO-mediated knockdown efficiency potentially through co-delivery or treatment with activators of autophagy. Unlike the development of novel lytic peptide vectors or potentially toxic carrier systems, appropriate fasting paradigms, specific high-fat ketogenic diets, or other autophagy-enhancing diets would be a more convenient, safe, and flexible approach to enhancing oligonucleotide therapeutic activity. More broadly, these findings ultimately underscore the importance of understanding ASO trafficking in models and diseases where autophagy and lysosomal storage networks are altered and suggest that when developing oligonucleotide therapeutics, the status of autophagy in the disease state should also be taken into consideration when characterizing oligonucleotide molecules.

SUPPLEMENTARY DATA

Supplementary Data are available at NAR Online.

ACKNOWLEDGEMENTS

We wish to thank Dr Frank Bennett, Dr Brett Monia, and Dr Shiyu Wang for stimulating discussions; Gemma Ebeling for experimental and technical assistance; Tracy Reigle and Wanda Sullivan for graphics support.

FUNDING

Internal funding from Ionis Pharmaceuticals. Funding for open access charge: Ionis Pharmaceuticals internal funding.
Conflict of interest statement. J.O., A.F.P., S.Gr., N.M.P., J.E.M., A.R.M., S.Gu. and M.A. are employees and shareholders of Ionis Pharmaceuticals.

REFERENCES

1. Schoch,K.M. and Miller,T.M. (2017) Antisense oligonucleotides: translation from mouse models to human neurodegenerative diseases. *Neuron*, **94**, 1056–1070.
2. Shen,X. and Corey,D.R. (2018) Chemistry, mechanism and clinical status of antisense oligonucleotides and duplex RNAs. *Nucleic Acids Res.*, **46**, 1584–1600.
3. Beltinger,C., Saragovi,H.U., Smith,R.M., LeSauteur,L., Shah,N., DeDionisio,L., Christensen,L., Raible,A., Jarett,L. and Gewirtz,A.M. (1995) Binding, uptake, and intracellular trafficking of phosphorothioate-modified oligodeoxynucleotides. *J. Clin. Invest.*, **95**, 1814–1823.
4. Geary,R.S., Norris,D., Yu,R. and Bennett,C.F. (2015) Pharmacokinetics, biodistribution and cell uptake of antisense oligonucleotides. *Adv. Drug. Deliv. Rev.*, **87**, 46–51.
5. Crooke,S.T., Wang,S., Vickers,T.A., Shen,W. and Liang,X.H. (2017) Cellular uptake and trafficking of antisense oligonucleotides. *Nat. Biotechnol.*, **35**, 230–237.
6. Miller,C.M., Donner,A.J., Blank,E.E., Egger,A.W., Kellar,B.M., Ostergaard,M.E., Seth,P.P. and Harris,E.N. (2016) Stabilin-1 and Stabilin-2 are specific receptors for the cellular internalization of phosphorothioate-modified antisense oligonucleotides (ASOs) in the liver. *Nucleic Acids Res.*, **44**, 2782–2794.
7. Juliano,R.L. (2016) The delivery of therapeutic oligonucleotides. *Nucleic Acids Res.*, **44**, 6518–6548.
8. Tooze,S.A., Abada,A. and Elazar,Z. (2014) Endocytosis and autophagy: exploitation or cooperation? *Cold Spring Harb. Perspect. Biol.*, **6**, a018358.
9. Yu,L., Chen,Y. and Tooze,S.A. (2018) Autophagy pathway: Cellular and molecular mechanisms. *Autophagy*, **14**, 207–215.
10. Shibutani,S.T. and Yoshimori,T. (2014) A current perspective of autophagosome biogenesis. *Cell Res.*, **24**, 58–68.
11. Kim,Y.C. and Guan,K.L. (2015) mTOR: a pharmacologic target for autophagy regulation. *J. Clin. Invest.*, **125**, 25–32.
12. Jung,C.H., Ro,S.H., Cao,J., Otto,N.M. and Kim,D.H. (2010) mTOR regulation of autophagy. *FEBS Lett.*, **584**, 1287–1295.
13. Martina,J.A., Chen,Y., Gucek,M. and Puertollano,R. (2012) MTORC1 functions as a transcriptional regulator of autophagy by preventing nuclear transport of TFEB. *Autophagy*, **8**, 903–914.
14. Settembre,C., Di Malta,C., Polito,V.A., Garcia Arencibia,M., Vetrini,F., Erdin,S., Erdin,S.U., Huynh,T., Medina,D., Colella,P. *et al.* (2011) TFEB links autophagy to lysosomal biogenesis. *Science*, **332**, 1429–1433.
15. Nnah,I.C., Wang,B., Saqcena,C., Weber,G.F., Bonder,E.M., Bagley,D., De Cegli,R., Napolitano,G., Medina,D.L., Ballabio,A. *et al.* (2019) TFEB-driven endocytosis coordinates MTORC1 signaling and autophagy. *Autophagy*, **15**, 151–164.
16. Napolitano,G. and Ballabio,A. (2016) TFEB at a glance. *J. Cell Sci.*, **129**, 2475–2481.

17. Song,W., Ma,Z., Zhang,Y. and Yang,C. (2017) Autophagy plays a dual role during intracellular siRNA delivery by lipoplex and polyplex nanoparticles. *Acta Biomater.*, **58**, 196–204.
18. Zhong,X., Panus,D., Ji,W. and Wang,C. (2015) Modulating polyplex-mediated gene transfection by small-molecule regulators of autophagy. *Mol. Pharm.*, **12**, 932–940.
19. Dowaidar,M., Gestin,M., Cerrato,C.P., Jafferali,M.H., Margus,H., Kivistik,P.A., Ezzat,K., Hallberg,E., Pooga,M., Hallbrink,M. *et al.* (2017) Role of autophagy in cell-penetrating peptide transfection model. *Sci. Rep.*, **7**, 12635.
20. Man,N., Chen,Y., Zheng,F., Zhou,W. and Wen,L.P. (2010) Induction of genuine autophagy by cationic lipids in mammalian cells. *Autophagy*, **6**, 449–454.
21. Cardarelli,F., Digiacomo,L., Marchini,C., Amici,A., Salomone,F., Fiume,G., Rossetta,A., Gratton,E., Pozzi,D. and Caracciolo,G. (2016) The intracellular trafficking mechanism of Lipofectamine-based transfection reagents and its implication for gene delivery. *Sci. Rep.*, **6**, 25879.
22. Mui,B., Ahkong,Q.F., Chow,L. and Hope,M.J. (2000) Membrane perturbation and the mechanism of lipid-mediated transfer of DNA into cells. *Biochim. Biophys. Acta*, **1467**, 281–292.
23. Mo,R.H., Zaro,J.L., Ou,J.H. and Shen,W.C. (2012) Effects of Lipofectamine 2000/siRNA complexes on autophagy in hepatoma cells. *Mol. Biotechnol.*, **51**, 1–8.
24. Seth,P.P., Vasquez,G., Allerson,C.A., Berdeja,A., Gaus,H., Kinberger,G.A., Prakash,T.P., Migawa,M.T., Bhat,B. and Swayze,E.E. (2010) Synthesis and biophysical evaluation of 2′,4′-constrained 2′O-methoxyethyl and 2′,4′-constrained 2′O-ethyl nucleic acid analogues. *J. Org. Chem.*, **75**, 1569–1581.
25. Hung,G., Xiao,X., Peralta,R., Bhattacharjee,G., Murray,S., Norris,D., Guo,S. and Monia,B.P. (2013) Characterization of target mRNA reduction through in situ RNA hybridization in multiple organ systems following systemic antisense treatment in animals. *Nucleic Acid Ther.*, **23**, 369–378.
26. Zhang,B., Arun,G., Mao,Y.S., Lazar,Z., Hung,G., Bhattacharjee,G., Xiao,X., Booth,C.J., Wu,J., Zhang,C. *et al.* (2012) The lncRNA Malat1 is dispensable for mouse development but its transcription plays a cis-regulatory role in the adult. *Cell Rep.*, **2**, 111–123.
27. Tanowitz,M., Hettrick,L., Revenko,A., Kinberger,G.A., Prakash,T.P. and Seth,P.P. (2017) Asialoglycoprotein receptor 1 mediates productive uptake of N-acetylgalactosamine-conjugated and unconjugated phosphorothioate antisense oligonucleotides into liver hepatocytes. *Nucleic Acids Res.*, **45**, 12388–12400.
28. Wang,S., Sun,H., Tanowitz,M., Liang,X.H. and Crooke,S.T. (2016) Annexin A2 facilitates endocytic trafficking of antisense oligonucleotides. *Nucleic Acids Res.*, **44**, 7314–7330.
29. Koller,E., Vincent,T.M., Chappell,A., De,S., Manoharan,M. and Bennett,C.F. (2011) Mechanisms of single-stranded phosphorothioate modified antisense oligonucleotide accumulation in hepatocytes. *Nucleic Acids Res.*, **39**, 4795–4807.
30. Sini,P., James,D., Chresta,C. and Guichard,S. (2010) Simultaneous inhibition of mTORC1 and mTORC2 by mTOR kinase inhibitor AZD8055 induces autophagy and cell death in cancer cells. *Autophagy*, **6**, 553–554.
31. Honda,A., Harrington,E., Cornella-Taracido,I., Furet,P., Knapp,M.S., Glick,M., Triantafellow,E., Dowdle,W.E., Wiedershain,D., Maniara,W. *et al.* (2016) Potent, Selective, and Orally Bioavailable Inhibitors of VPS34 Provide Chemical Tools to Modulate Autophagy in Vivo. *ACS Med. Chem. Lett.*, **7**, 72–76.
32. Mauthe,M., Orhon,I., Rocchi,C., Zhou,X., Luhr,M., Hijlkema,K.J., Coppes,R.P., Engedal,N., Mari,M. and Reggiori,F. (2018) Chloroquine inhibits autophagic flux by decreasing autophagosome-lysosome fusion. *Autophagy*, **14**, 1435–1455.
33. Sarkar,S., Davies,J.E., Huang,Z., Tunnacliffe,A. and Rubinsztein,D.C. (2007) Trehalose, a novel mTOR-independent autophagy enhancer, accelerates the clearance of mutant huntingtin and alpha-synuclein. *J. Biol. Chem.*, **282**, 5641–5652.
34. Kimura,T., Jia,J., Claude-Taupin,A., Kumar,S., Choi,S.W., Gu,Y., Mudd,M., Dupont,N., Jiang,S., Peters,R. *et al.* (2017) Cellular and molecular mechanism for secretory autophagy. *Autophagy*, **13**, 1084–1085.
35. Seth,P.P., Siwkowski,A., Allerson,C.R., Vasquez,G., Lee,S., Prakash,T.P., Wancewicz,E.V., Witchell,D. and Swayze,E.E. (2009) Short antisense oligonucleotides with novel 2′–4′ conformationaly restricted nucleoside analogues show improved potency without increased toxicity in animals. *J. Med. Chem.*, **52**, 10–13.
36. Filomeni,G., De Zio,D. and Cecconi,F. (2015) Oxidative stress and autophagy: the clash between damage and metabolic needs. *Cell Death Differ.*, **22**, 377–388.
37. Pasquier,B. (2015) SAR405, a PIK3C3/Vps34 inhibitor that prevents autophagy and synergizes with MTOR inhibition in tumor cells. *Autophagy*, **11**, 725–726.
38. Arakawa,S., Honda,S., Yamaguchi,H. and Shimizu,S. (2017) Molecular mechanisms and physiological roles of Atg5/Atg7-independent alternative autophagy. *Proc. Jpn. Acad. Ser. B Phys. Biol. Sci.*, **93**, 378–385.
39. Kuma,A., Komatsu,M. and Mizushima,N. (2017) Autophagy-monitoring and autophagy-deficient mice. *Autophagy*, **13**, 1619–1628.
40. Moulis,M. and Vindis,C. (2017) Methods for measuring autophagy in mice. *Cells*, **6**, E14.
41. Roberts,M.N., Wallace,M.A., Tomilov,A.A., Zhou,Z., Marcotte,G.R., Tran,D., Perez,G., Gutierrez-Casado,E., Koike,S., Knotts,T.A. *et al.* (2017) A ketogenic diet extends longevity and healthspan in adult mice. *Cell Metab.*, **26**, 539–546.
42. Roberts,M.N., Wallace,M.A., Tomilov,A.A., Zhou,Z., Marcotte,G.R., Tran,D., Perez,G., Gutierrez-Casado,E., Koike,S., Knotts,T.A. *et al.* (2018) A ketogenic diet extends longevity and healthspan in adult mice. *Cell Metab.*, **27**, 1156.
43. Liang,X.H., Sun,H., Nichols,J.G., Allen,N., Wang,S., Vickers,T.A., Shen,W., Hsu,C.W. and Crooke,S.T. (2018) COPII vesicles can affect the activity of antisense oligonucleotides by facilitating the release of oligonucleotides from endocytic pathways. *Nucleic Acids Res.*, **46**, 10225–10245.
44. Mejlvang,J., Olsvik,H., Svenning,S., Bruun,J.A., Abudu,Y.P., Larsen,K.B., Brech,A., Hansen,T.E., Brenne,H., Hansen,T. *et al.* (2018) Starvation induces rapid degradation of selective autophagy receptors by endosomal microautophagy. *J. Cell Biol.*, **217**, 3640–3655.
45. Muller,M., Schmidt,O., Angelova,M., Faserl,K., Weys,S., Kremser,L., Pfaffenwimmer,T., Dalik,T., Kraft,C., Trajanoski,Z. *et al.* (2015) The coordinated action of the MVB pathway and autophagy ensures cell survival during starvation. *Elife*, **4**, e07736.
46. Karanasios,E., Stapleton,E., Manifava,M., Kaizuka,T., Mizushima,N., Walker,S.A. and Ktistakis,N.T. (2013) Dynamic association of the ULK1 complex with omegasomes during autophagy induction. *J. Cell Sci.*, **126**, 5224–5238.
47. Hyttinen,J.M., Niittykoski,M., Salminen,A. and Kaarniranta,K. (2013) Maturation of autophagosomes and endosomes: a key role for Rab7. *Biochim. Biophys. Acta*, **1833**, 503–510.
48. Haobam,B., Nozawa,T., Minowa-Nozawa,A., Tanaka,M., Oda,S., Watanabe,T., Aikawa,C., Maruyama,F. and Nakagawa,I. (2014) Rab17-mediated recycling endosomes contribute to autophagosome formation in response to Group A Streptococcus invasion. *Cell. Microbiol.*, **16**, 1806–1821.
49. Longatti,A. and Tooze,S.A. (2012) Recycling endosomes contribute to autophagosome formation. *Autophagy*, **8**, 1682–1683.
50. Jager,S., Bucci,C., Tanida,I., Ueno,T., Kominami,E., Saftig,P. and Eskelinen,E.L. (2004) Role for Rab7 in maturation of late autophagic vacuoles. *J. Cell Sci.*, **117**, 4837–4848.
51. Bissig,C. and Gruenberg,J. (2013) Lipid sorting and multivesicular endosome biogenesis. *Cold Spring Harb. Perspect. Biol.*, **5**, a016816.
52. Punnonen,E.L., Autio,S., Kaija,H. and Reunanen,H. (1993) Autophagic vacuoles fuse with the prelysosomal compartment in cultured rat fibroblasts. *Eur. J. Cell Biol.*, **61**, 54–66.
53. Tooze,J., Hollinshead,M., Ludwig,T., Howell,K., Hoflack,B. and Kern,H. (1990) In exocrine pancreas, the basolateral endocytic pathway converges with the autophagic pathway immediately after the early endosome. *J. Cell Biol.*, **111**, 329–345.
54. Chan,S.N. and Tang,B.L. (2013) Location and membrane sources for autophagosome formation - from ER-mitochondria contact sites to Golgi-endosome-derived carriers. *Mol. Membr. Biol.*, **30**, 394–402.
55. Zhang,M., Wang,Y. and Ge,L. (2018) Endomembrane remodeling in autophagic membrane formation. *Autophagy*, **14**, 918–920.
56. Wei,Y., Liu,M., Li,X., Liu,J. and Li,H. (2018) Origin of the Autophagosome Membrane in Mammals. *Biomed. Res. Int.*, **2018**, 1012789.

57. Jahreiss,L., Menzies,F.M. and Rubinsztein,D.C. (2008) The itinerary of autophagosomes: from peripheral formation to kiss-and-run fusion with lysosomes. *Traffic*, **9**, 574–587.
58. Kimura,S., Noda,T. and Yoshimori,T. (2008) Dynein-dependent movement of autophagosomes mediates efficient encounters with lysosomes. *Cell Struct. Funct.*, **33**, 109–122.
59. Wang,S., Sun,H., Tanowitz,M., Liang,X.H. and Crooke,S.T. (2017) Intra-endosomal trafficking mediated by lysobisphosphatidic acid contributes to intracellular release of phosphorothioate-modified antisense oligonucleotides. *Nucleic Acids Res.*, **45**, 5309–5322.
60. Sun,K., Deng,W., Zhang,S., Cai,N., Jiao,S., Song,J. and Wei,L. (2013) Paradoxical roles of autophagy in different stages of tumorigenesis: protector for normal or cancer cells. *Cell Biosci.*, **3**, 35.
61. Barth,S., Glick,D. and Macleod,K.F. (2010) Autophagy: assays and artifacts. *J. Pathol.*, **221**, 117–124.
62. Liu,B., Oltvai,Z.N., Bayir,H., Silverman,G.A., Pak,S.C., Perlmutter,D.H. and Bahar,I. (2017) Quantitative assessment of cell fate decision between autophagy and apoptosis. *Sci. Rep.*, **7**, 17605.
63. McDaniel,S.S., Rensing,N.R., Thio,L.L., Yamada,K.A. and Wong,M. (2011) The ketogenic diet inhibits the mammalian target of rapamycin (mTOR) pathway. *Epilepsia*, **52**, e7–e11.